EQUATION OF STATE CONSTRAINTS THROUGH BINARY NEUTRON STAR MERGER ASTEROSEISMOLOGY

NIKOLAOS STERGIOULAS

main collaborators: A. BAUSWEIN, J. CLARK, T. JANKA

(HITS) (Georgia Tech) MPA

DEPARTMENT OF PHYSICS
ARISTOTLE UNIVERSITY OF THESSALONIKI

Paris, May 18, 2016

Neutron Stars

First neutron star detected almost 50 years ago. Still, the fundamental properties of matter in the core of neutron stars remain largely uncertain.

No accurate radius determination!

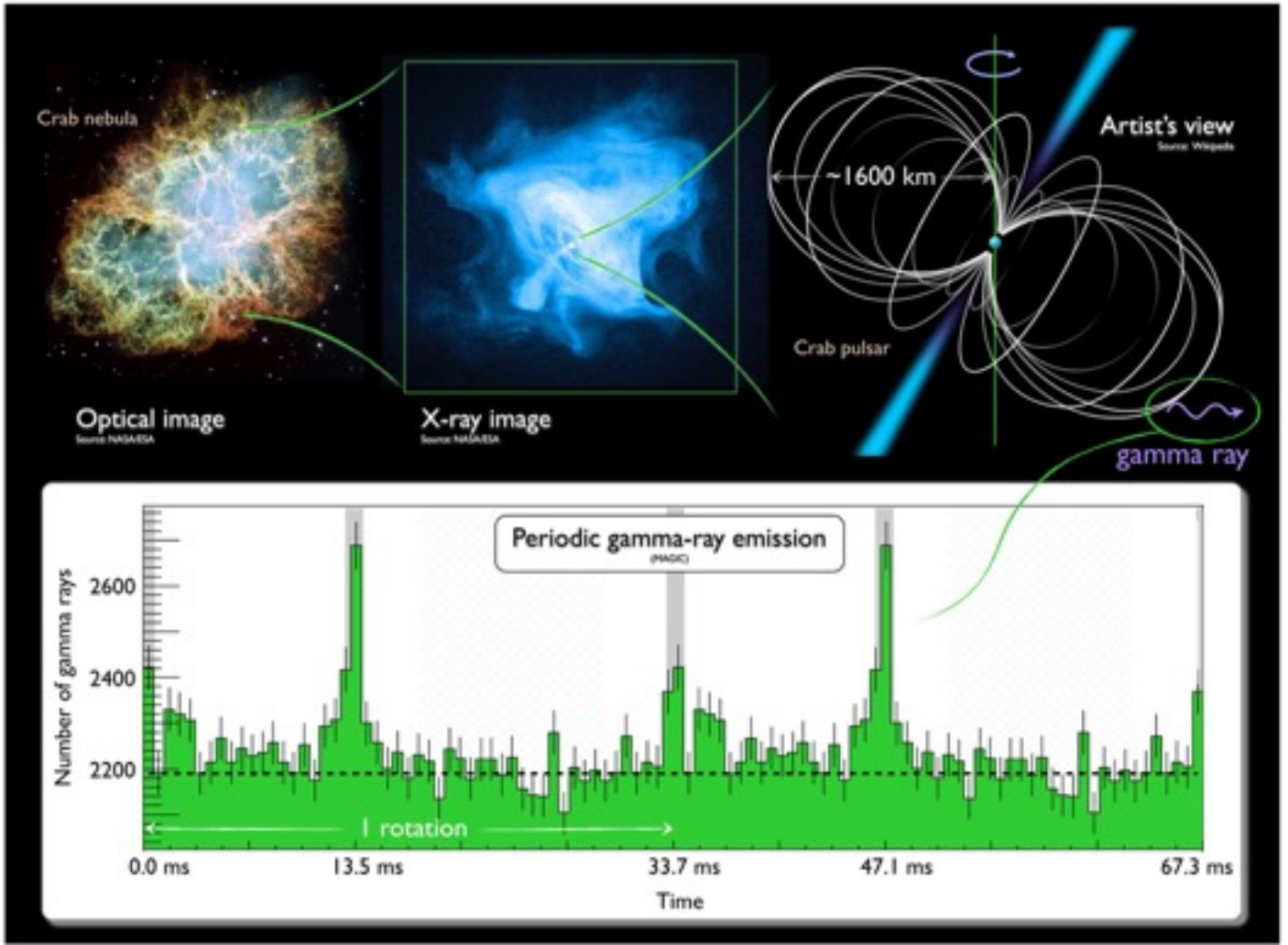

Image credit: MAGIC collaboration

Sample of Neutron Star Equations of State

Bauswein, Janka, Hebeler & Schwenk (2012)

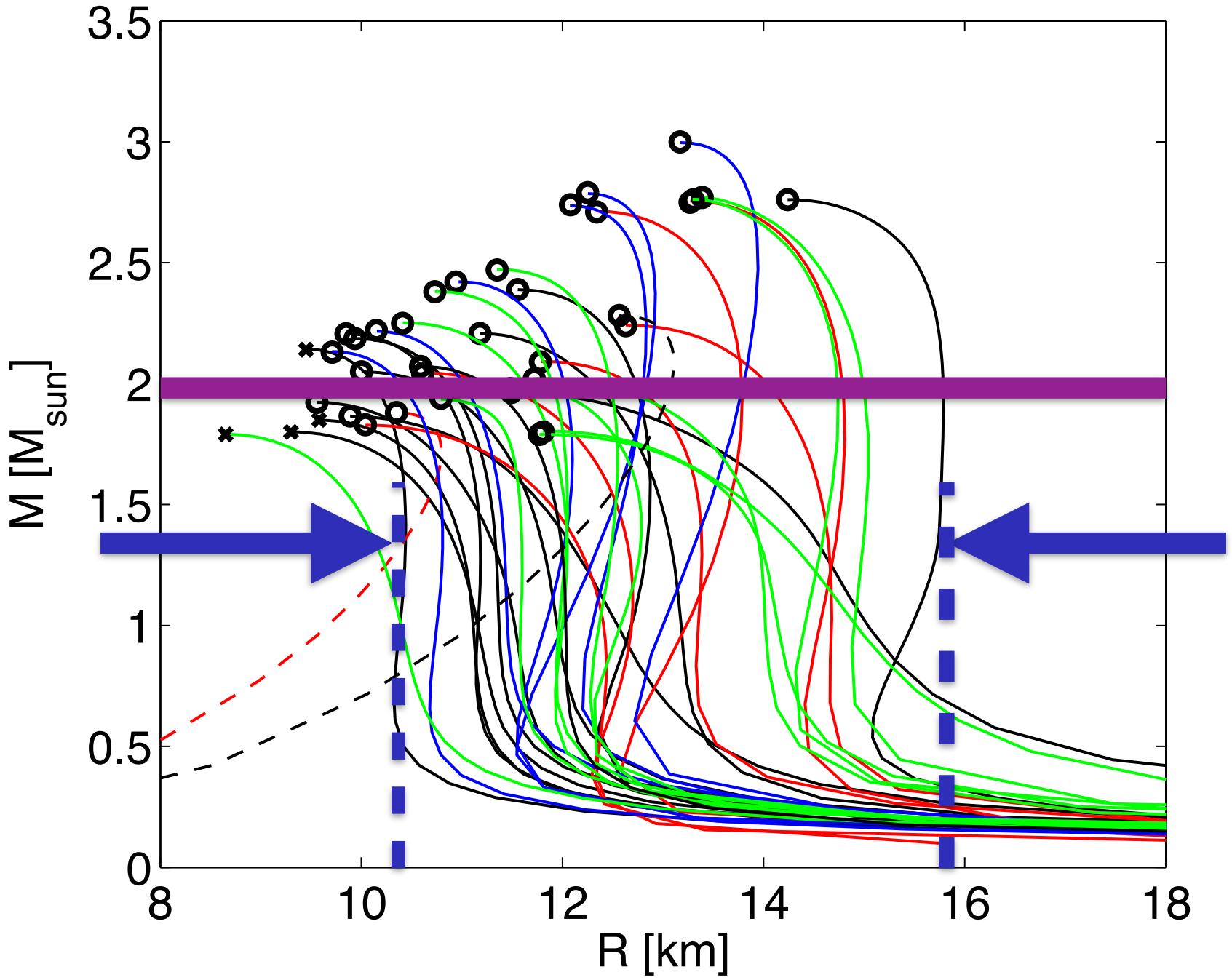

Constraints on Neutron Star Radii

Main methods in EM spectrum:

- Thermonuclear X-ray bursts (photospheric radius expansion)
- Burst oscillations (rotationally modulated waveform)
- Fits of thermal spectra to cooling neutron stars
- khZ QPOs in accretion disks around neutron stars
- Pericenter precession in relativistic binaries (double pulsar J0737)

Constraints from X-ray binaries / bursts

Oezel & Freire (2016)

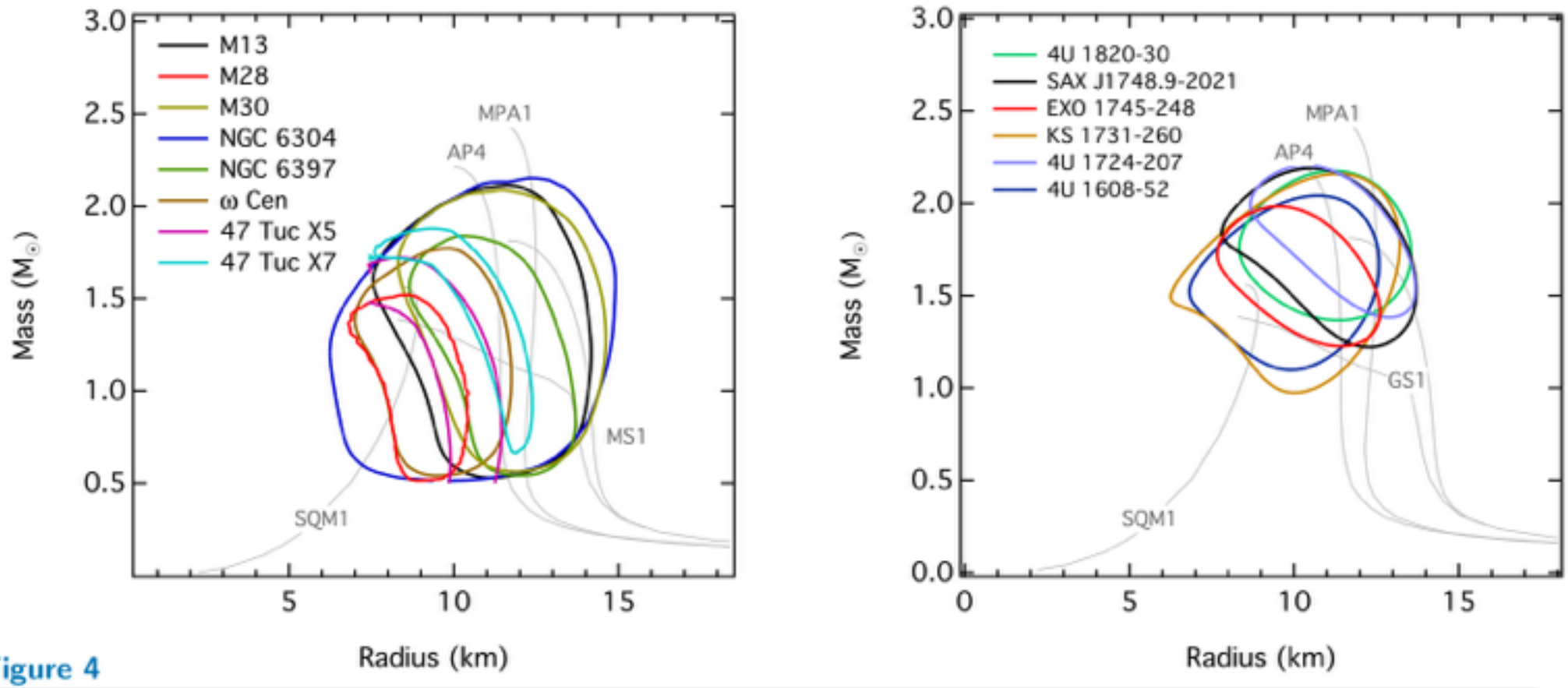

Figure 4

The combined constraints at the 68% confidence level over the neutron star mass and radius obtained from (Left) all neutron stars in low-mass X-ray binaries during quiescence (Right) all neutron stars with thermonuclear bursts. The light grey lines show mass-relations corresponding to a few representative equations of state (see Section 4.1 and Fig. 7 for detailed descriptions.)

Constraints on Neutron Star Radii

Main methods in EM spectrum:

- Thermonuclear X-ray bursts (photospheric radius expansion)
- Burst oscillations (rotationally modulated waveform)
- Fits of thermal spectra to cooling neutron stars
- khZ QPOs in accretion disks around neutron stars
- Pericenter precession in relativistic binaries (double pulsar J0737)

Main methods in GW spectrum:

- Tidal effects on waveform during inspiral phase of NS-NS mergers
- Tidal disruption in BH-NS mergers
- Oscillations in post-merger phase of NS-NS mergers

EOS from Inspiral Signal

Read et al. (2013)

The last part of the inspiral signal carries the imprint of the quadrupole *tidal deformability* $\lambda := -Q_{ij}/E_{ij} = 2/3\, k_2\, R^5$.

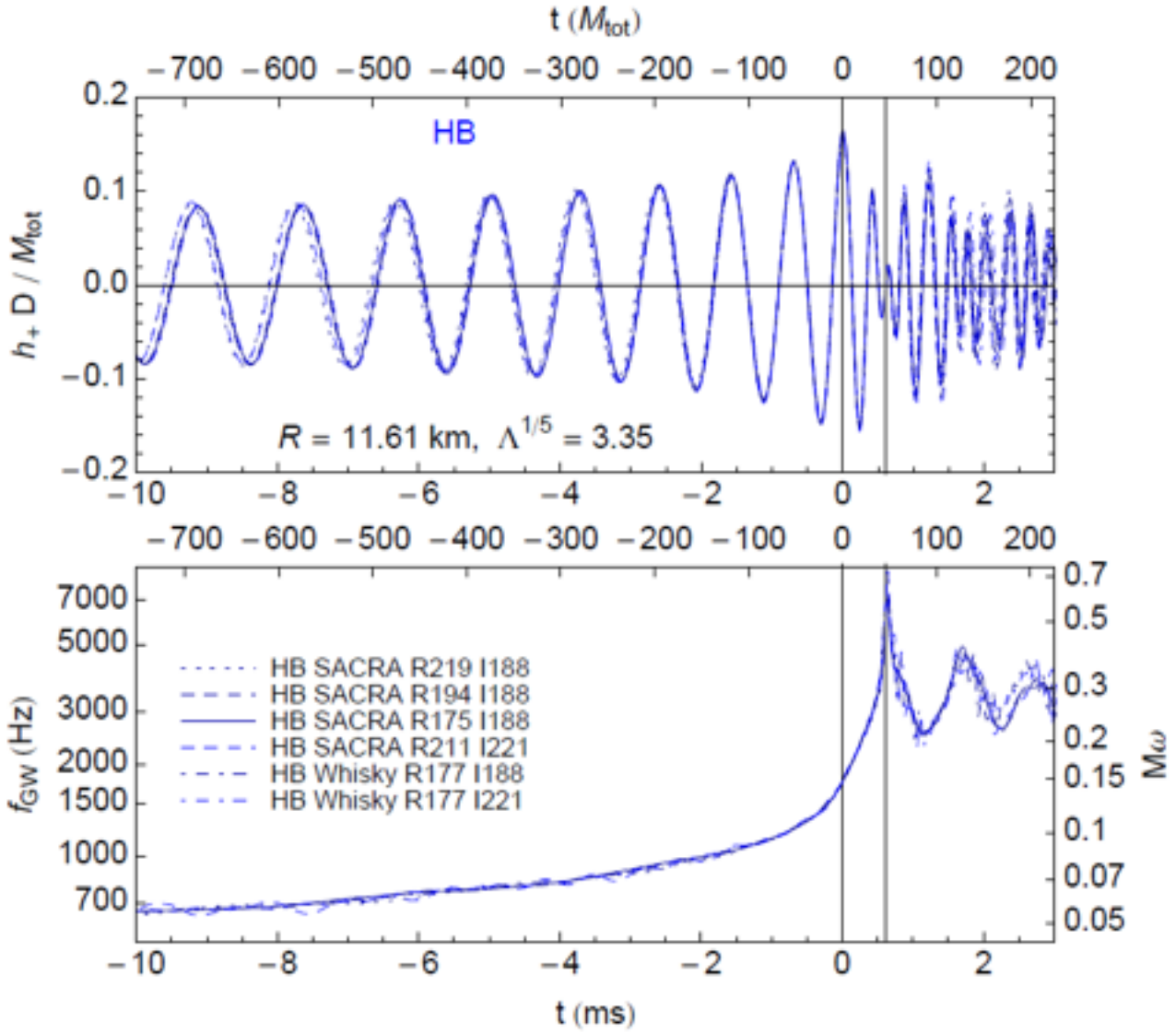

k_2 = tidal Love number

Dimensionless tidal deformability:

$$\Lambda \equiv \frac{2}{3} k_2 \left(\frac{R}{M}\right)^5$$

With an aLIGO class detector:

$\Delta R/R \sim 10\ \%$

@100 Mpc

Revealing the EOS

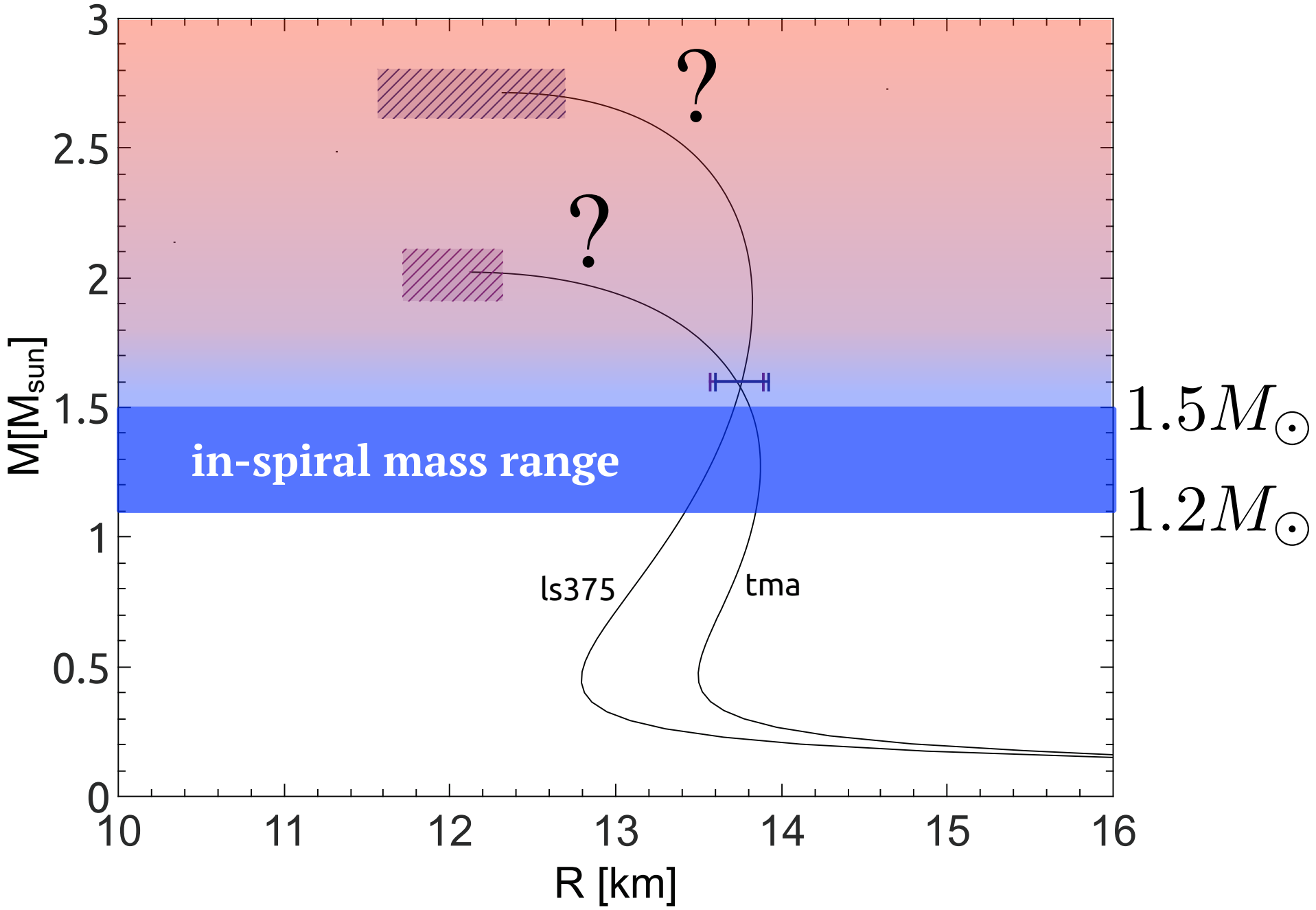

Outcome of Binary NS Mergers

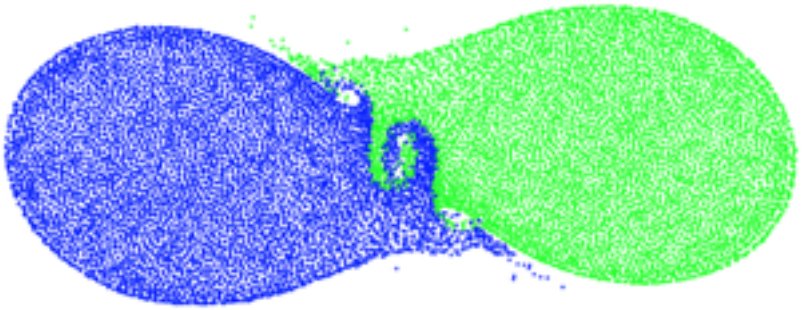

Most likely range of total mass for binary system:

$$2.4M_\odot < M_{\rm tot} < 3M_\odot$$

Because nonrotating $M_{\rm max} > 2M_\odot$ (as required by observations), a long-lived (τ >10ms) remnant is likely to be formed.

The remnant is a *hypermassive neutron star (HMNS)*, supported by *differential rotation*, with a mass larger than the maximum mass allowed for uniform rotation.

Simulations of BNS mergers

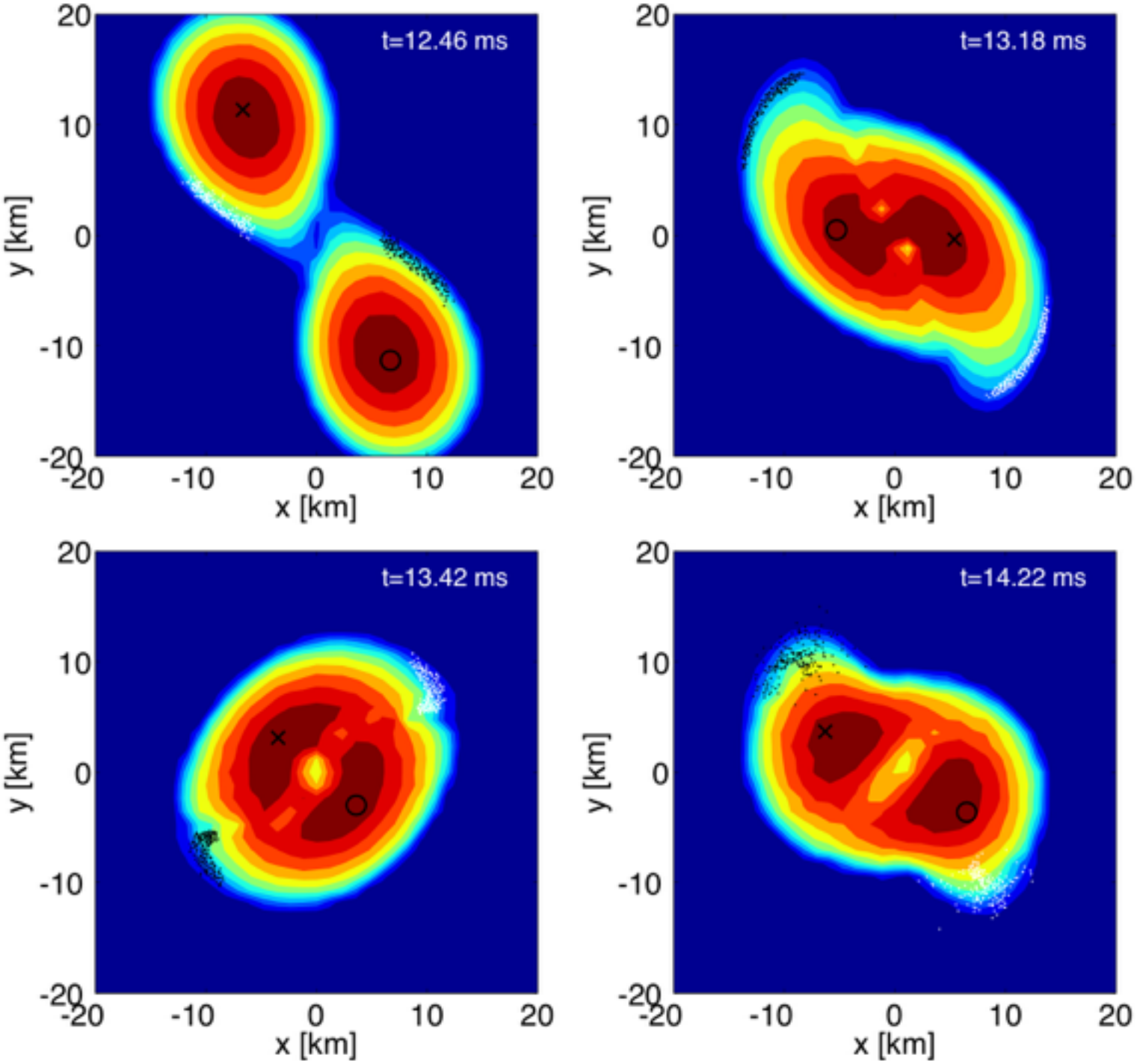

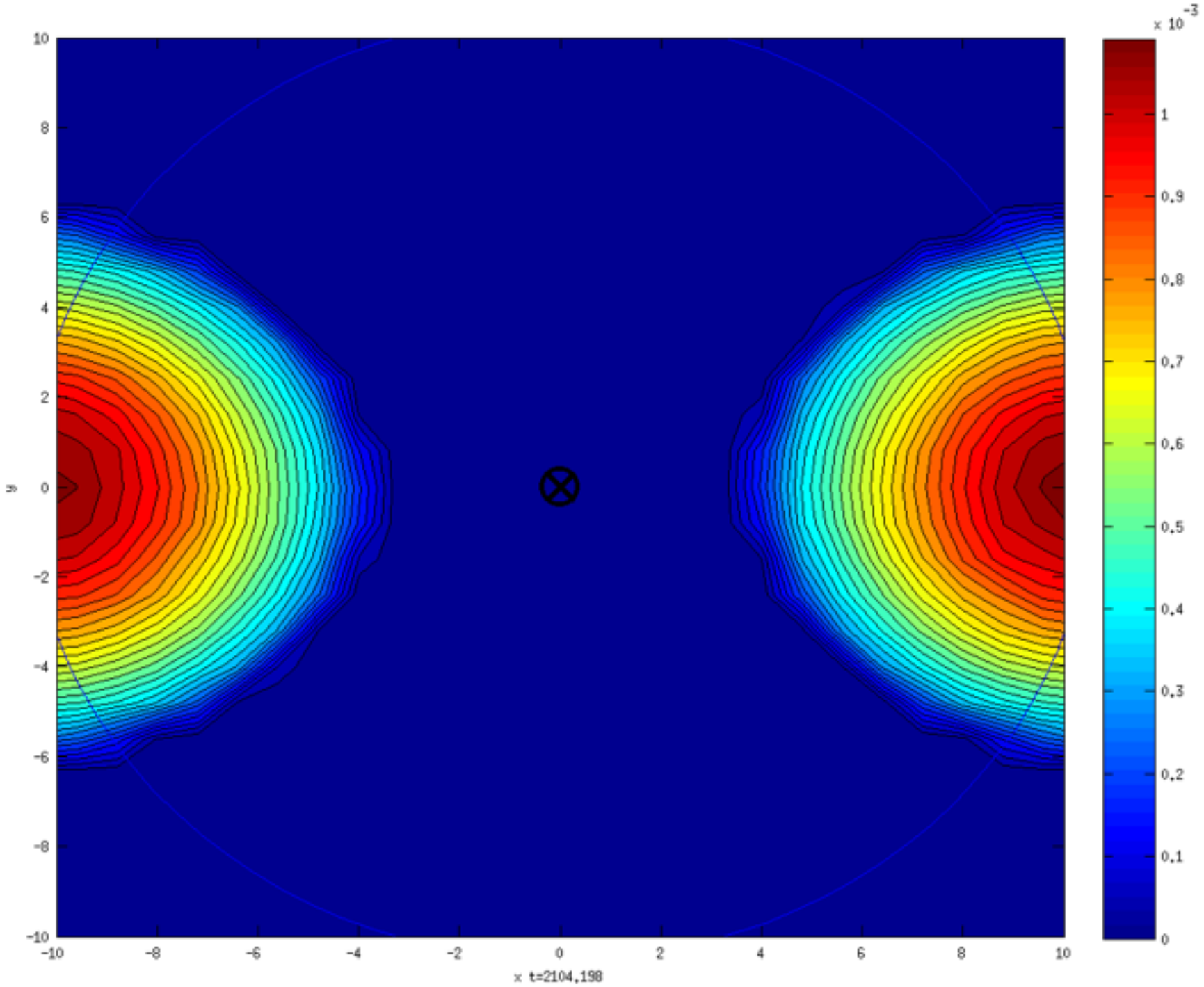
x 10^-3
1
0.9
0.8
0.7
0.6
0.5
0.4
0.3
0.2
0.1
0
10
8
6
4
2
0
-2
-4
-6
-8
-10
y
-10
-8
-6
-4
-2
0
2
4
6
8
10
x t=2104.198

Oscillations of Neutron Stars

$$\boldsymbol{\xi}(r,\theta,\phi) = \sum_{l=0}^{\infty} \sum_{m=-l}^{l} [U_l^m(r) Y_l^m(\theta,\phi)\hat{\mathbf{e}}_r + V_l^m(r)\nabla Y_l^m(\theta,\phi) + W_l^m(r)\hat{\mathbf{e}}_r \times \nabla Y_l^m(\theta,\phi)]$$

Main oscillation modes:

1. *f*-modes / *p*-modes

   fluid modes restored by pressure

2. *g*-modes

   restored by gravity/buoyancy

3. inertial modes (*r*-modes)

   restored by the Coriolis force in *rotating* stars

4. *w*-modes

   spacetime modes (similar to black hole modes)

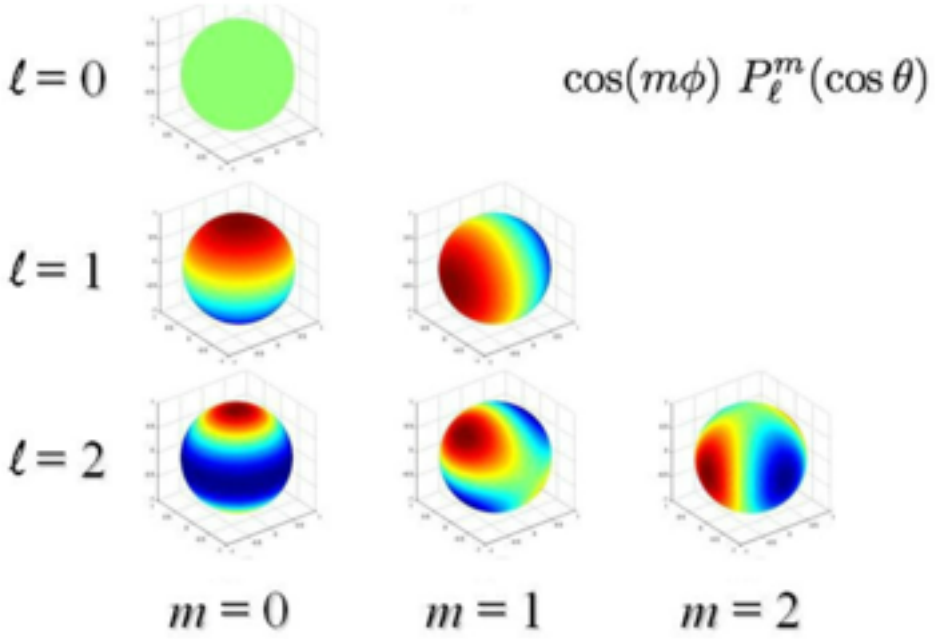

GW-detection: *f*-modes: stable oscillations

f-mode / *r*-mode *CFS*-instabilities

Post-Merger Gravitational Waves

NS, Bauswein, Zagkouris, Janks (2011)

The GW signal can be divided into three distinct phases:
inspiral, *merger* and *post-merger ringdown*. *(@40Mpc)*

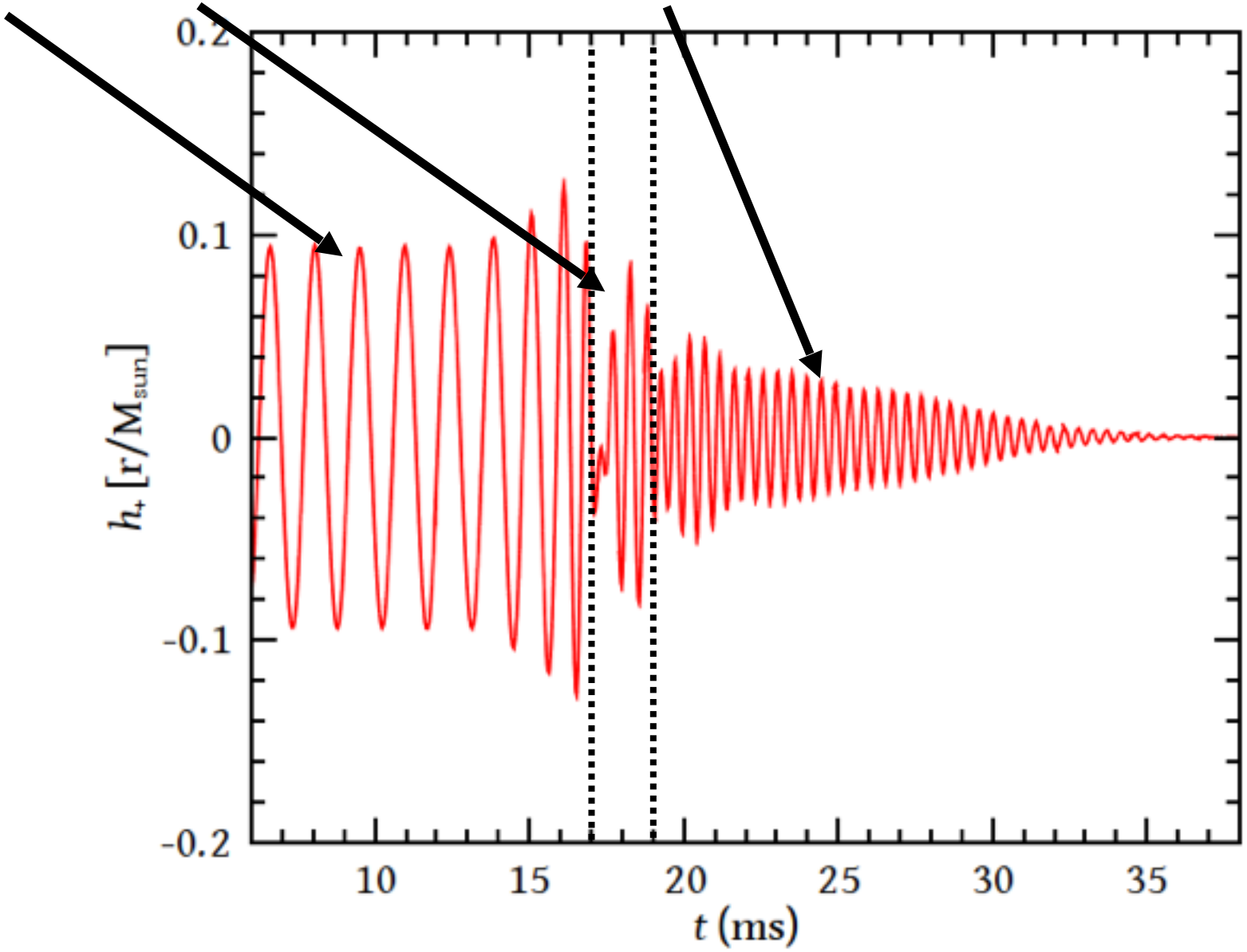

Post-Merger GW Spectrum

Several peaks stand above the aLIGO/VIRGO or ET sensitivity curves and are potentially detectable. How are these produced?

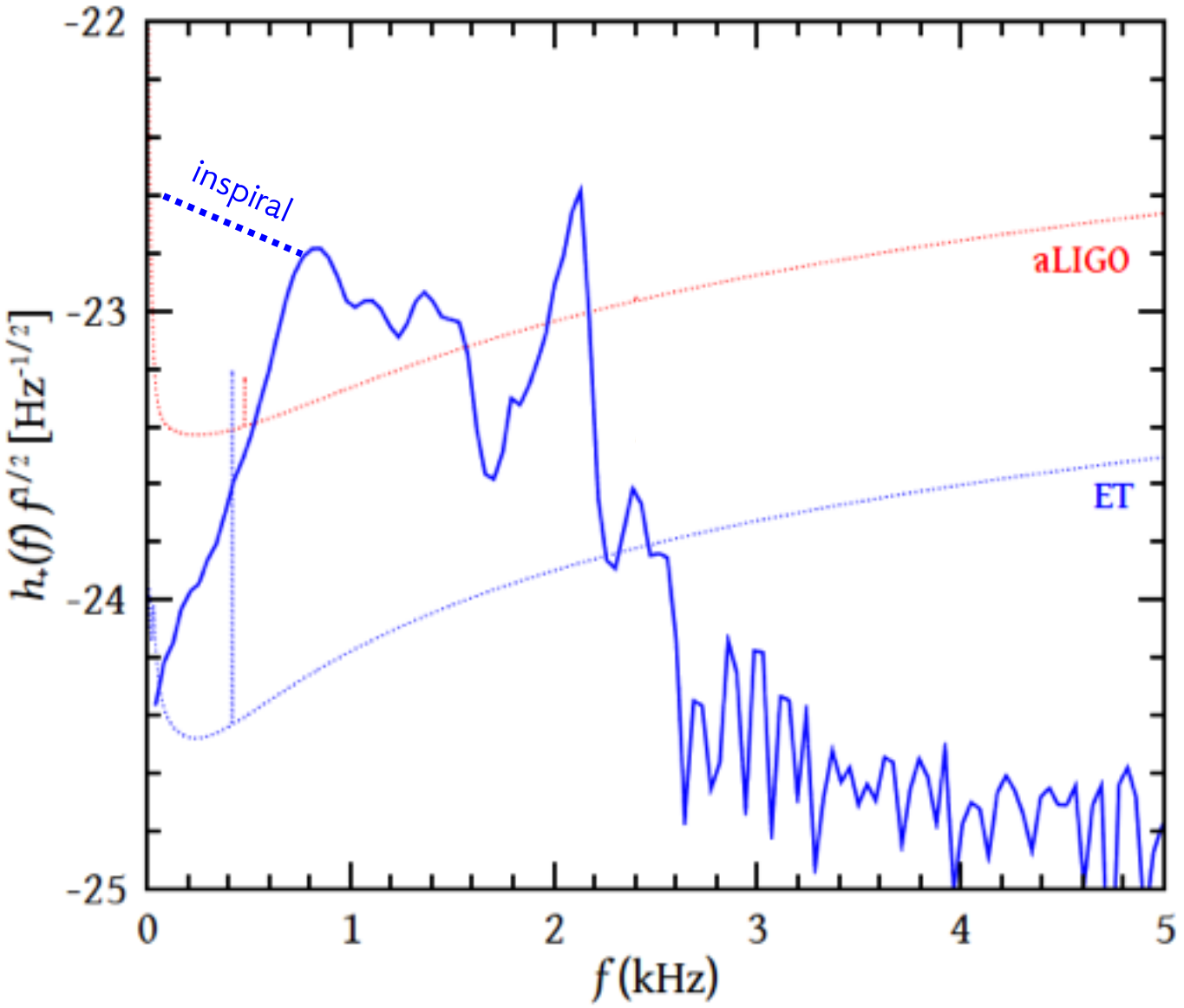

Lattimer-Swesty 220 EOS 1.35+1.35

GRAVITATIONAL WAVE SPECTRUM

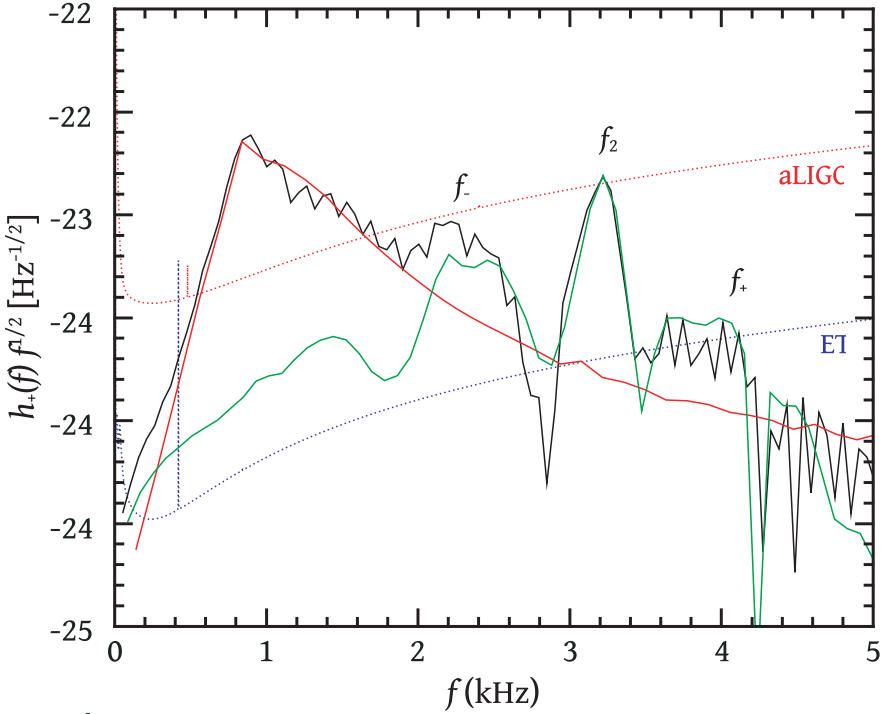

FFT OF HYDRODYNAMICS IN EQUATORIAL PLANE

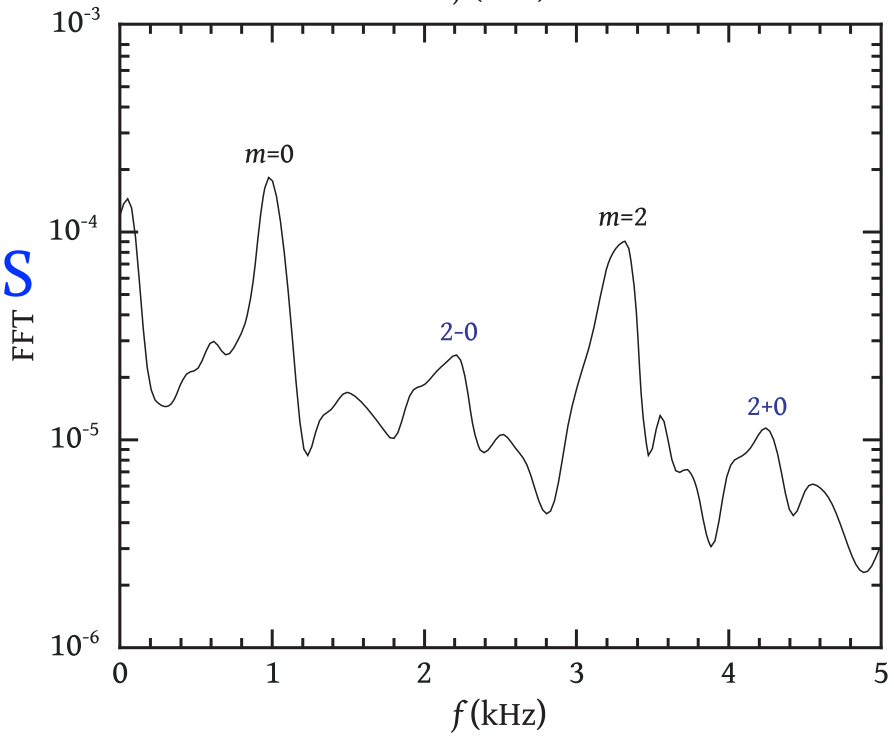

Lattimer-Swesty 220 EOS 1.35+1.35

GRAVITATIONAL WAVE SPECTRUM

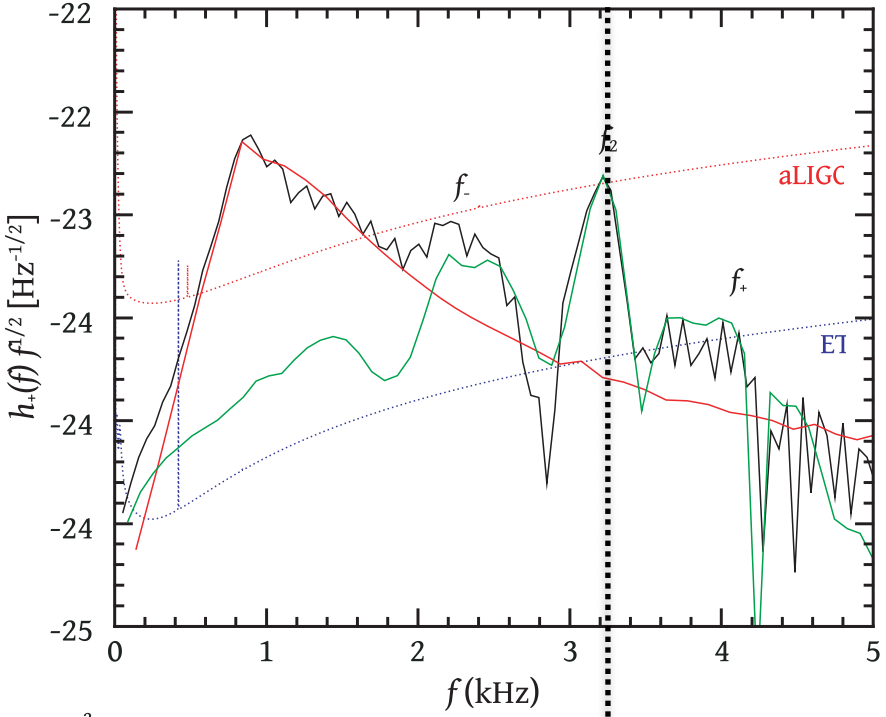

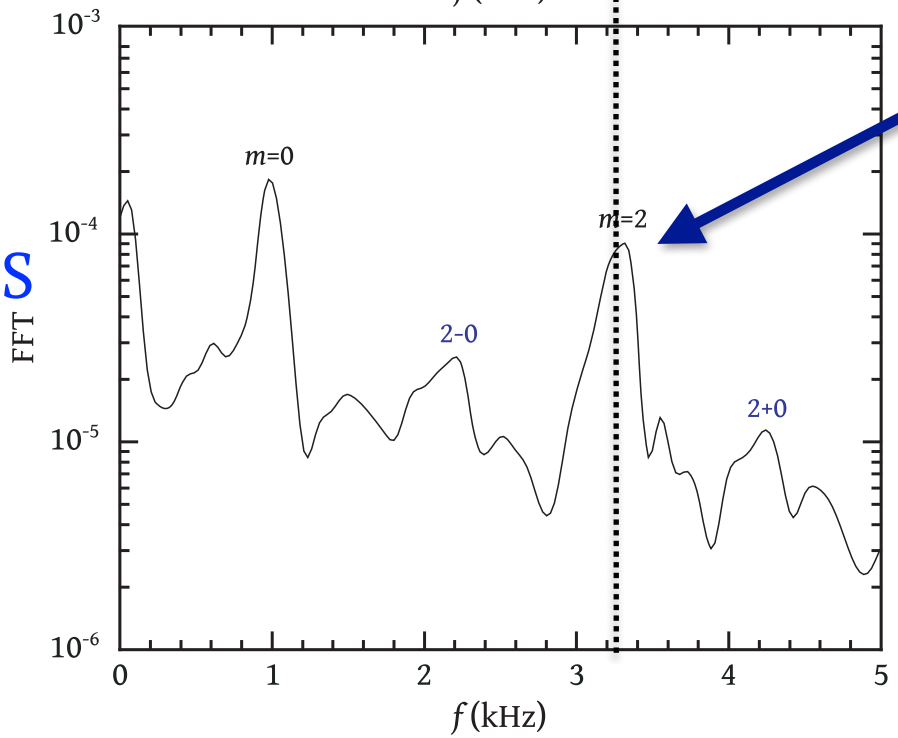

***l*=*m*=2**
linear f-mode

FFT OF HYDRODYNAMICS IN EQUATORIAL PLANE

Lattimer-Swesty 220 EOS 1.35+1.35

GRAVITATIONAL WAVE SPECTRUM

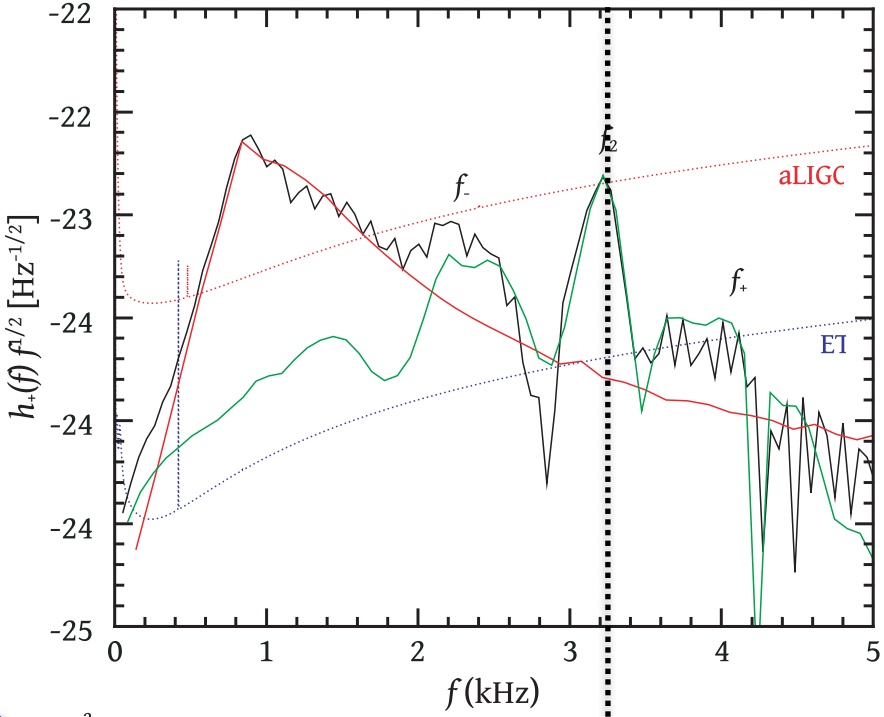

***l*=*m*=0 linear quasi-radial mode**

FFT OF HYDRODYNAMICS IN EQUATORIAL PLANE

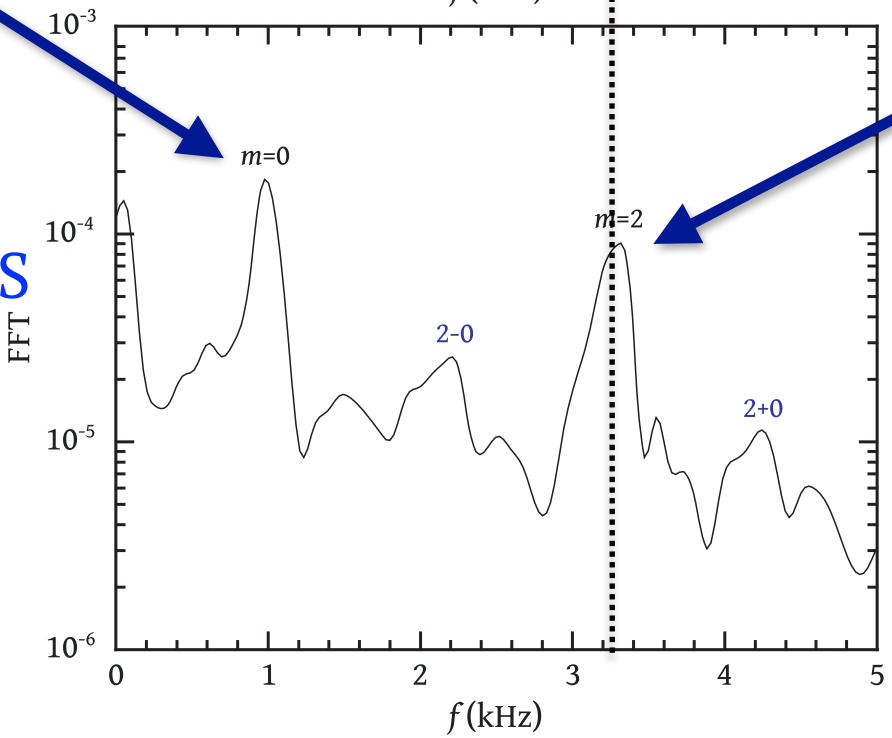

***l*=*m*=2 linear f-mode**

Lattimer-Swesty 220 EOS 1.35+1.35

GRAVITATIONAL WAVE SPECTRUM

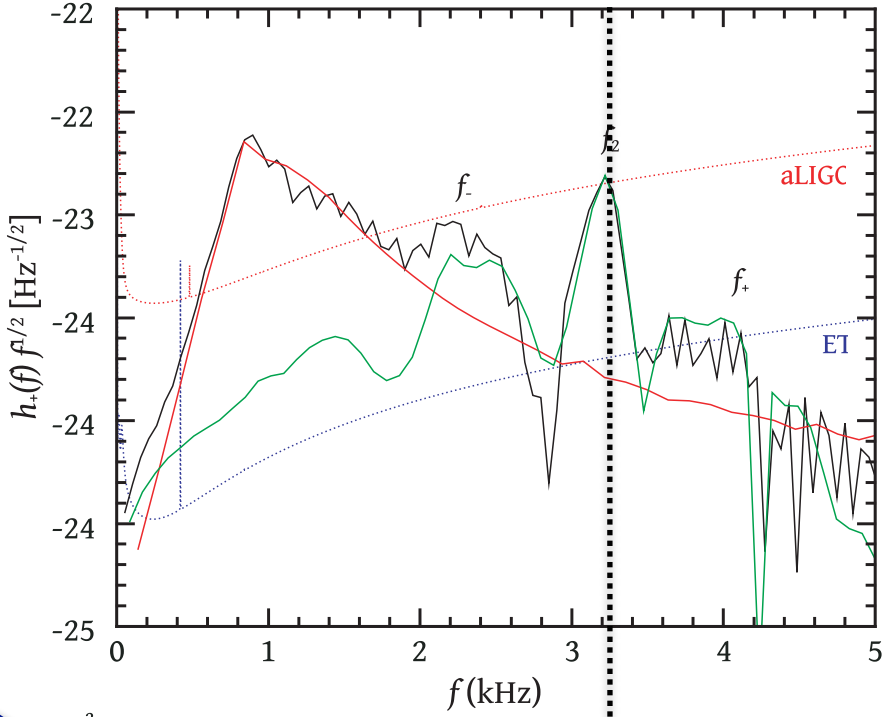

***l*=*m*=0 linear quasi-radial mode**

FFT OF HYDRODYNAMICS IN EQUATORIAL PLANE

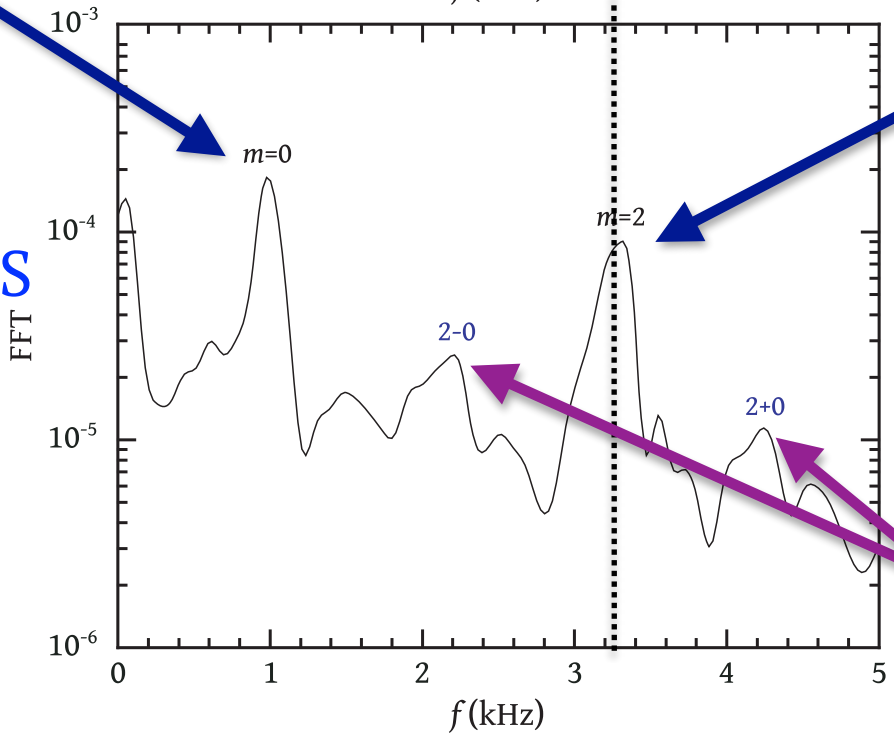

***l*=*m*=2 linear f-mode**

***"2-0" & "2+0" quasi-linear* combination frequencies**

Lattimer-Swesty 220 EOS 1.35+1.35

GRAVITATIONAL WAVE SPECTRUM

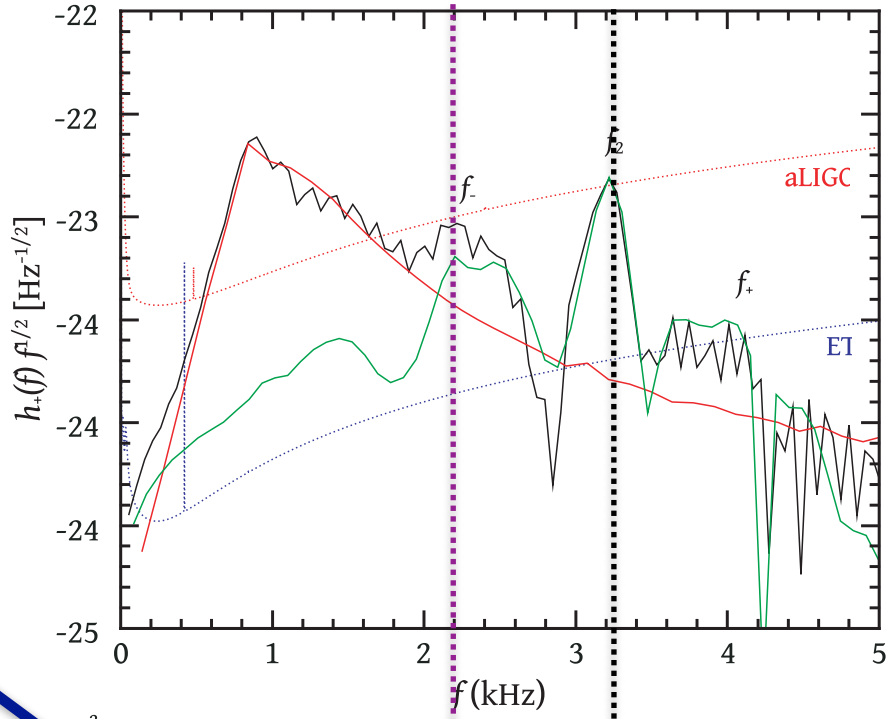

***l*=*m*=0 linear quasi-radial mode**

FFT OF HYDRODYNAMICS IN EQUATORIAL PLANE

***l*=*m*=2 linear f-mode**

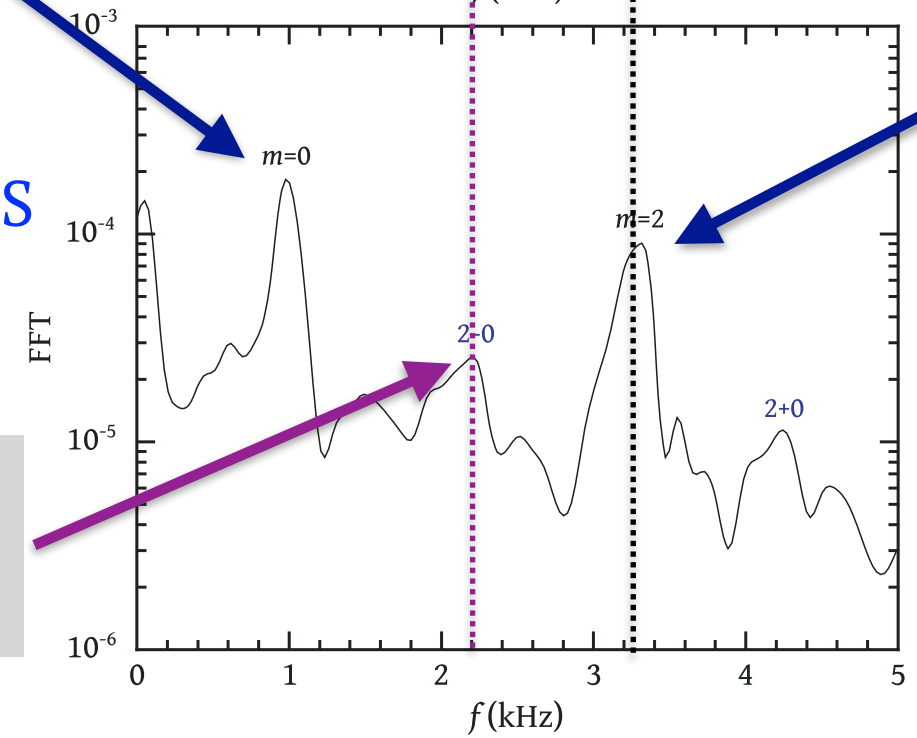

***"2-0" quasi-linear* combination frequency**

Tracing Individual Particles

Bauswein, NS (2015)

Using SPH it is simple to trace the paths of particles that originally belonged to one or the other star

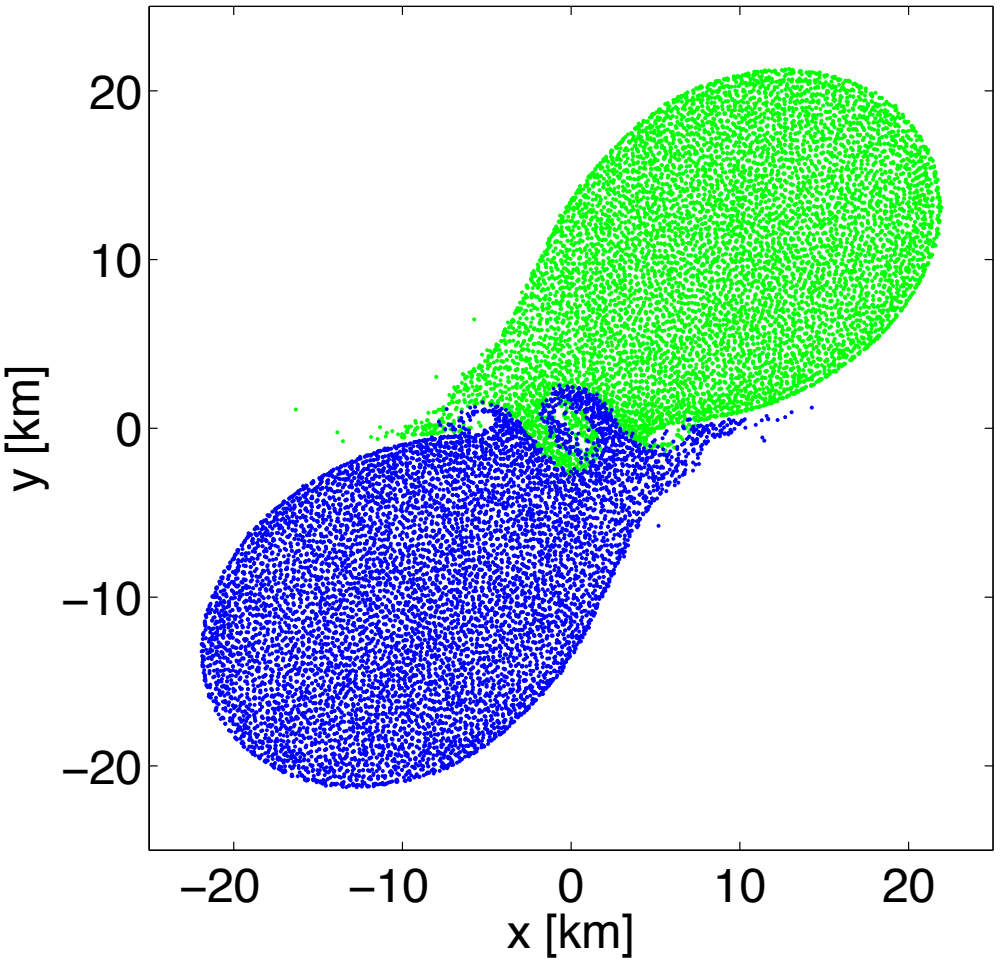

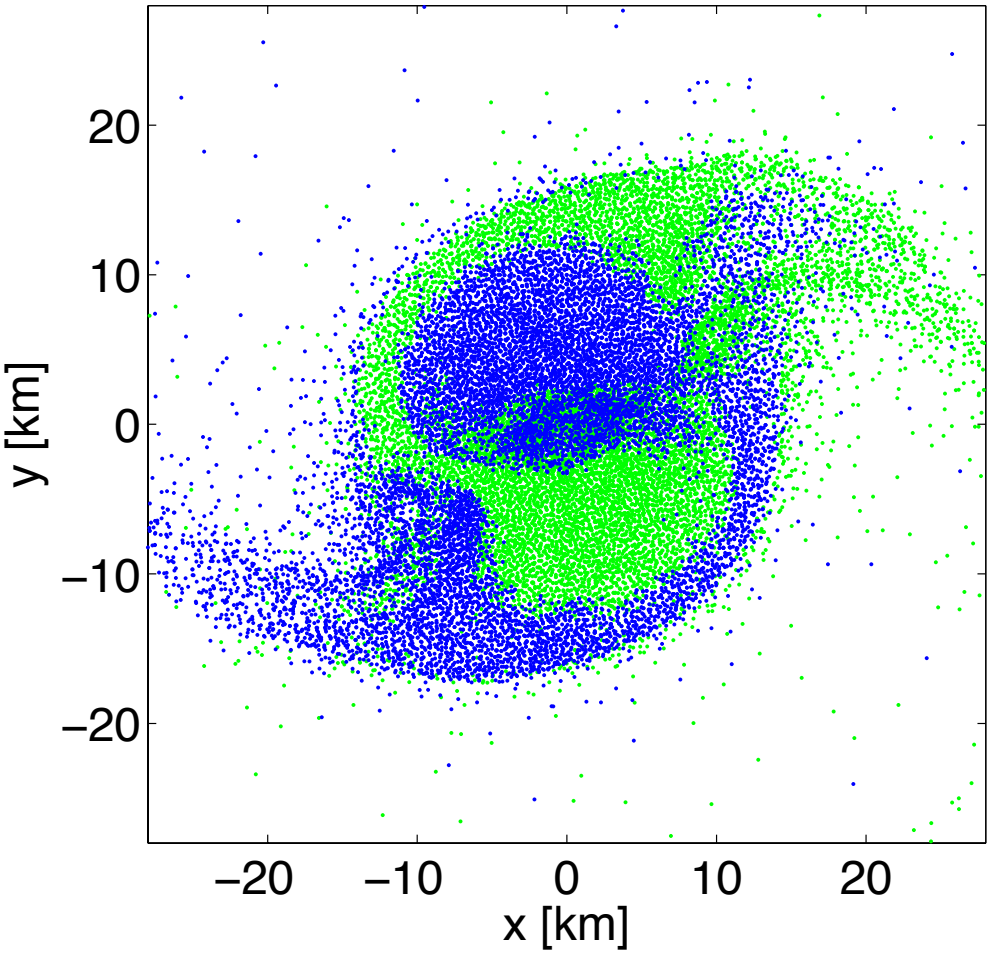

Spiral Deformation

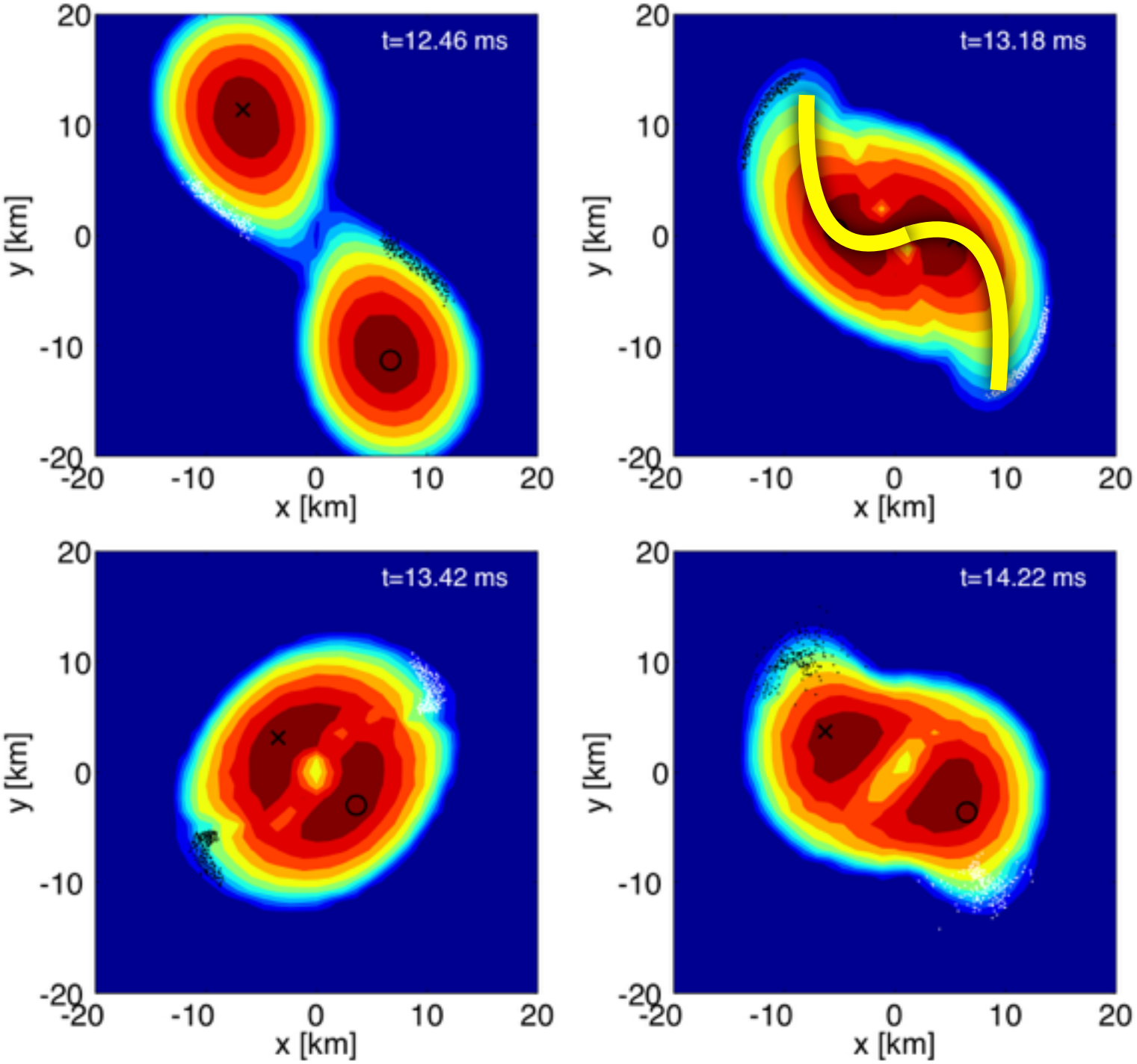

Lattimer-Swesty 220 EOS 1.35+1.35

GRAVITATIONAL WAVE SPECTRUM

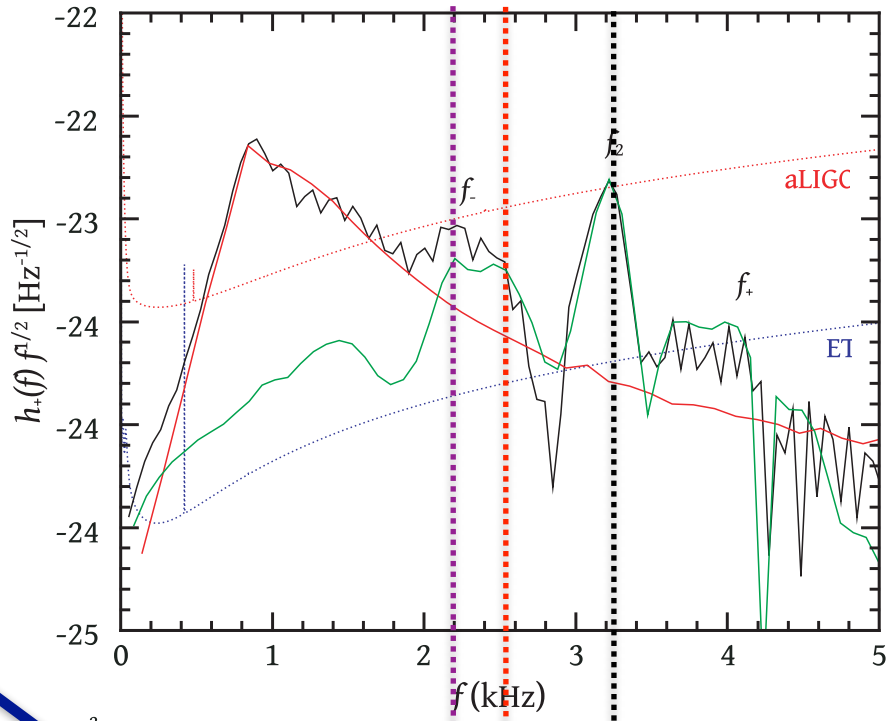

l=m=0 linear quasi-radial mode

FFT OF HYDRODYNAMICS IN EQUATORIAL PLANE

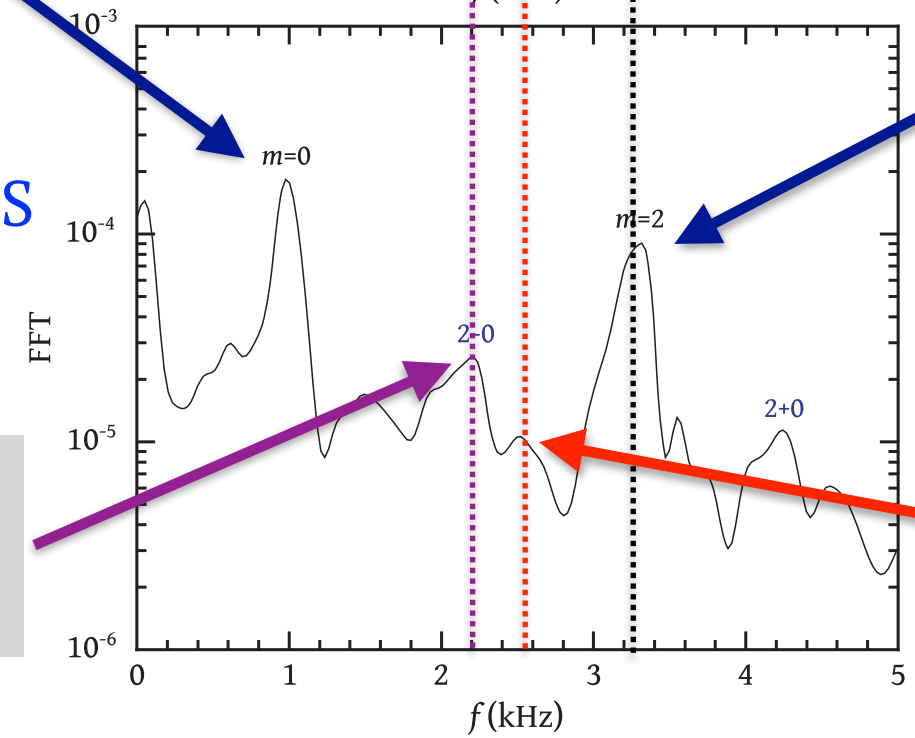

l=m=2 linear f-mode

***"2-0" quasi-linear* combination frequency**

***nonlinear* spiral frequency**

Time-Frequency Analysis

Clark, Bauswein, NS, Shoemaker (2016)

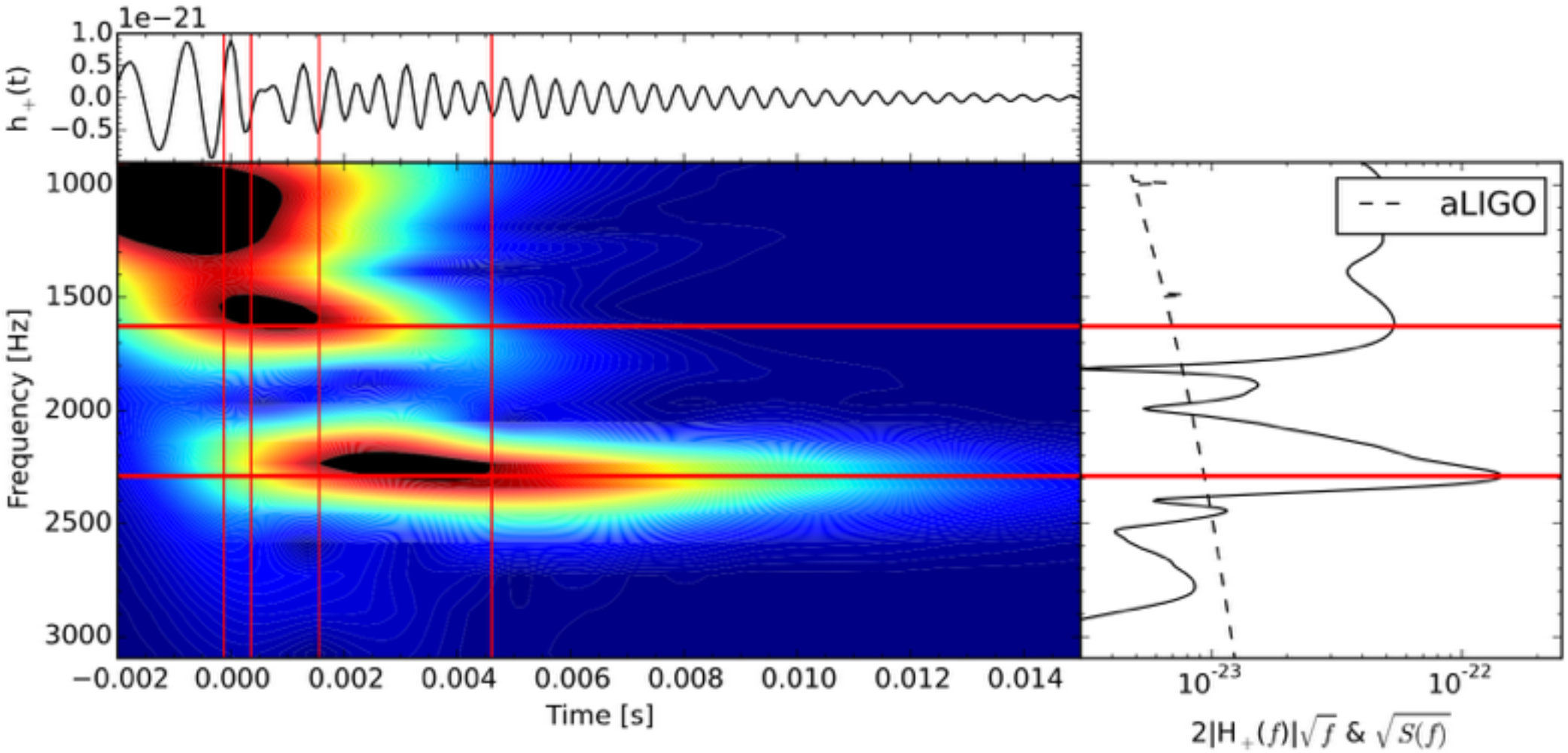

linear + quasi-linear + nonlinear

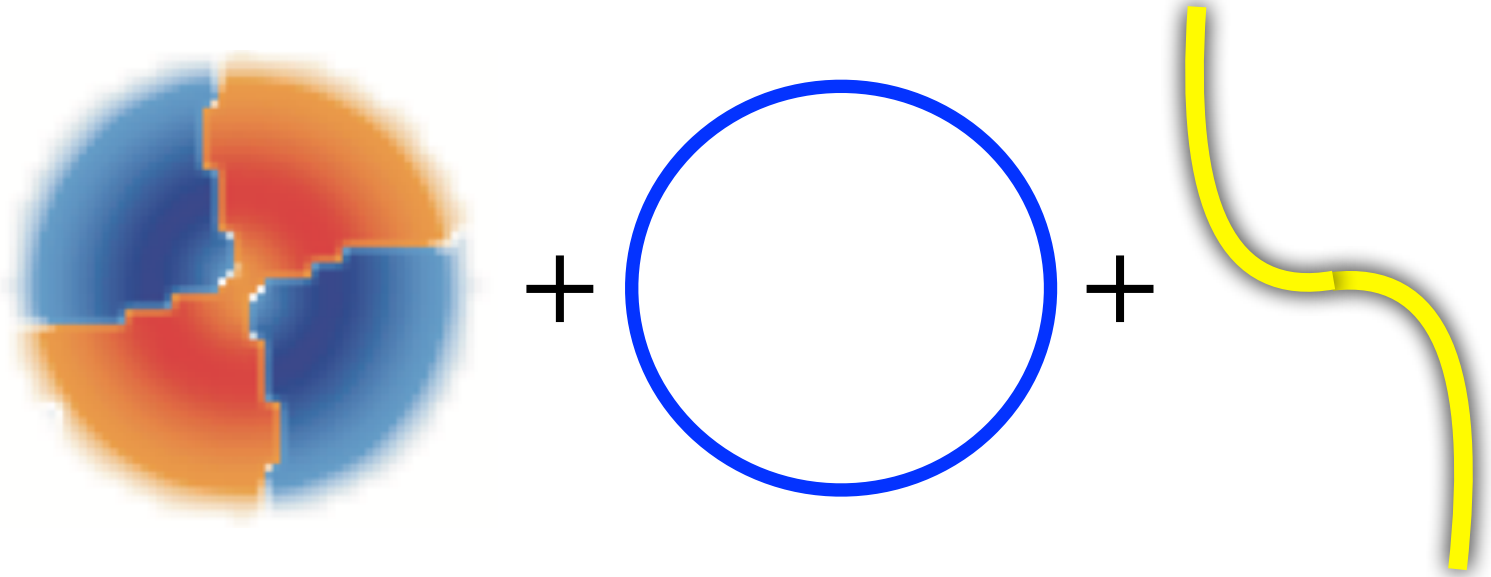

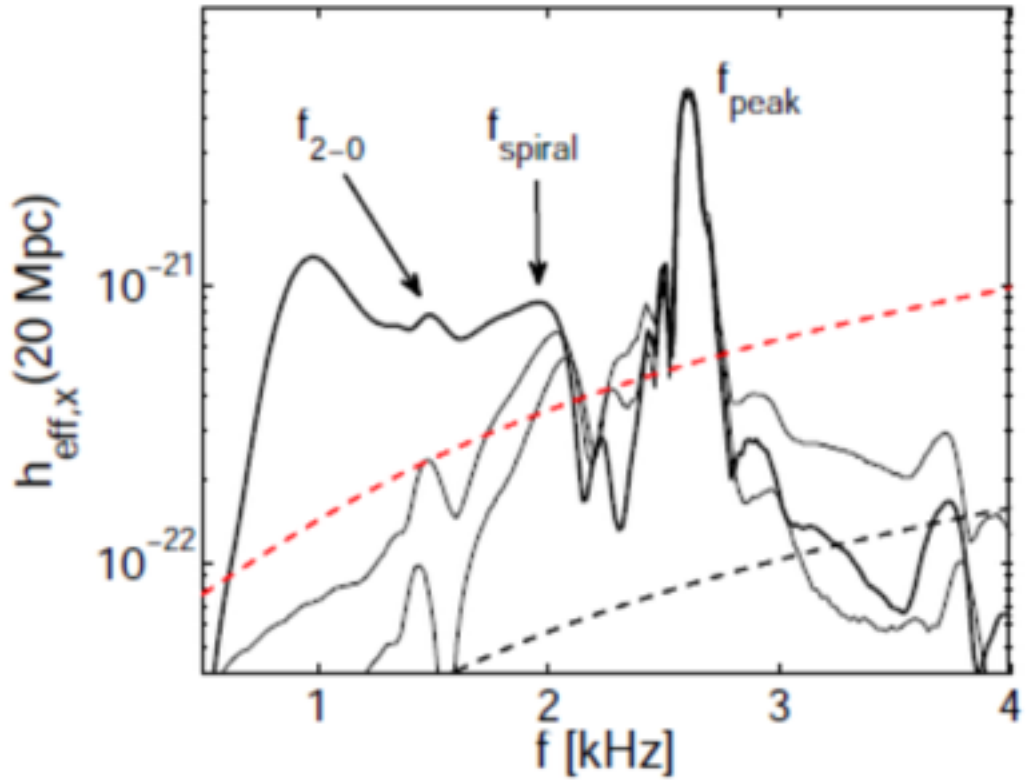

linear + quasi-linear + nonlinear

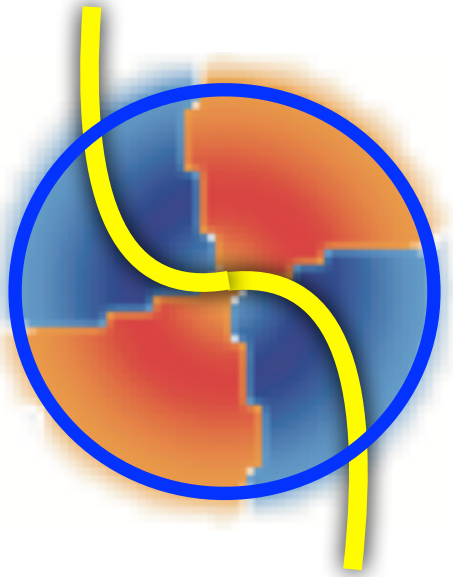

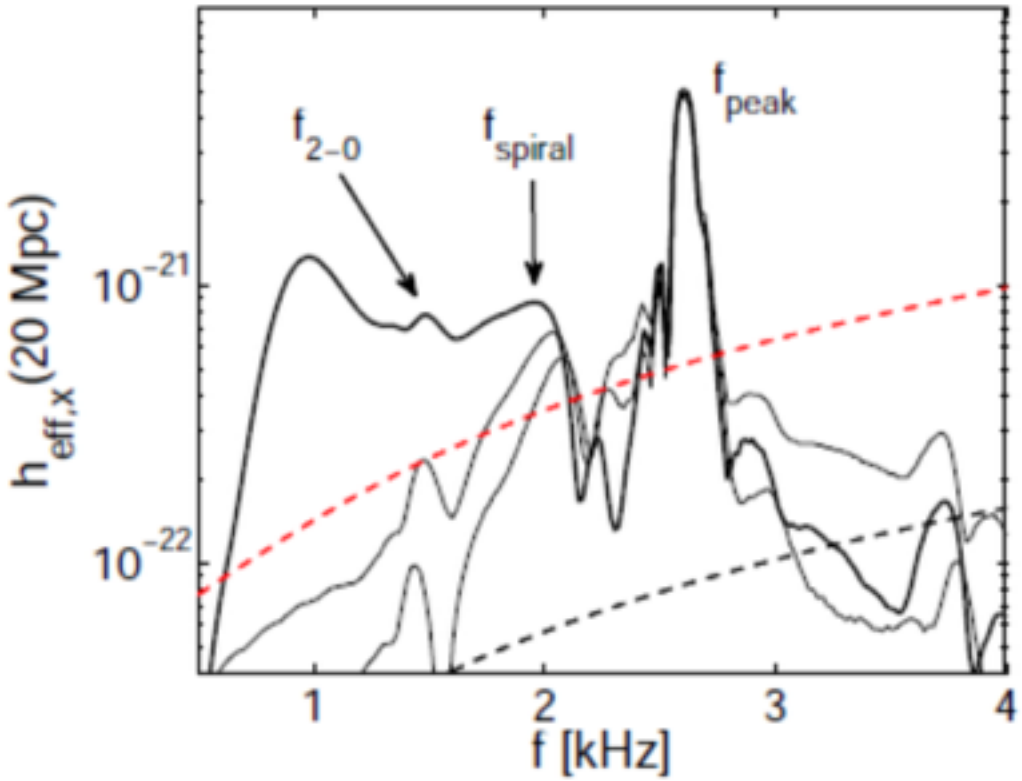

linear + quasi-linear + nonlinear

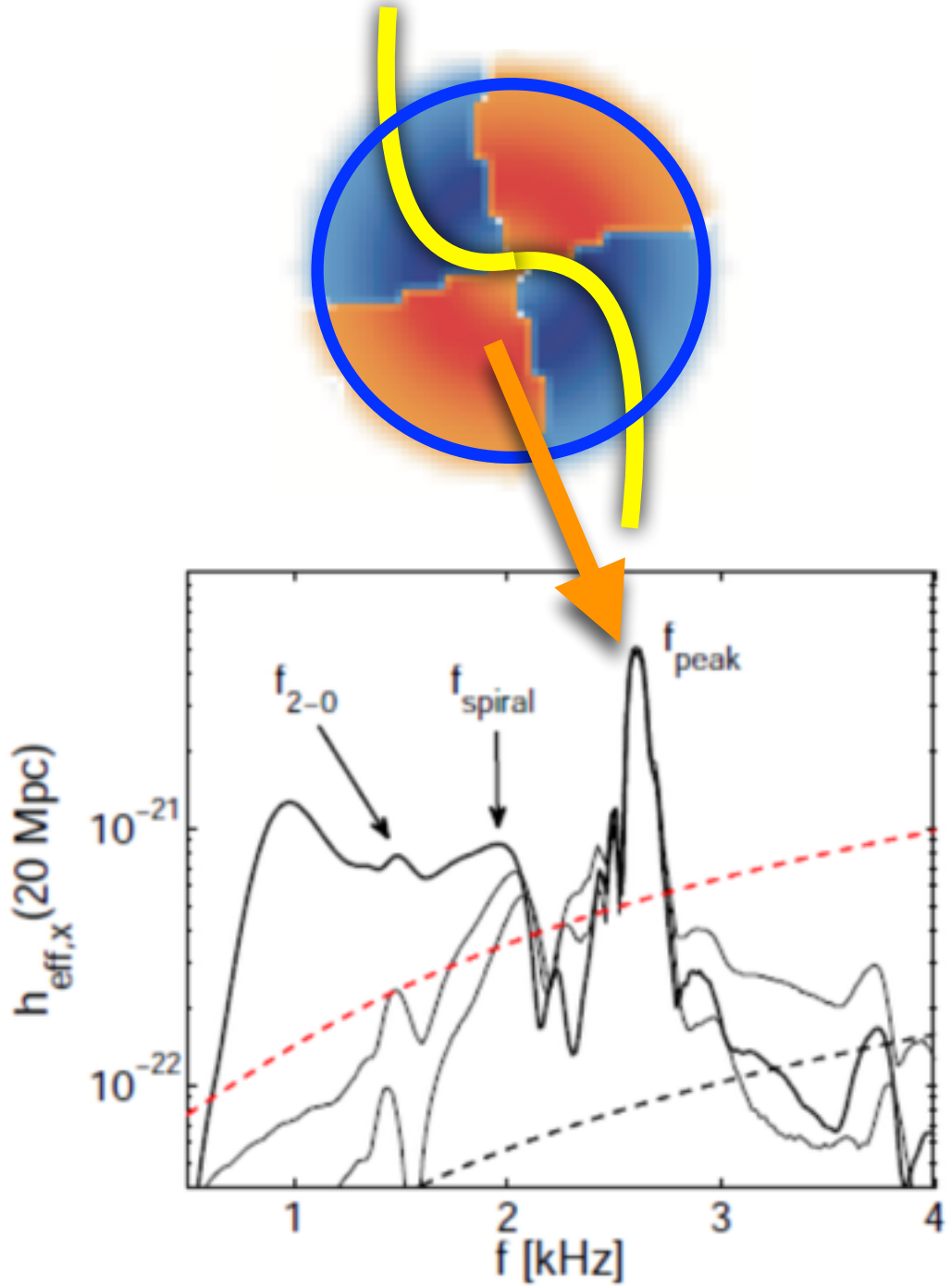

linear + quasi-linear + nonlinear

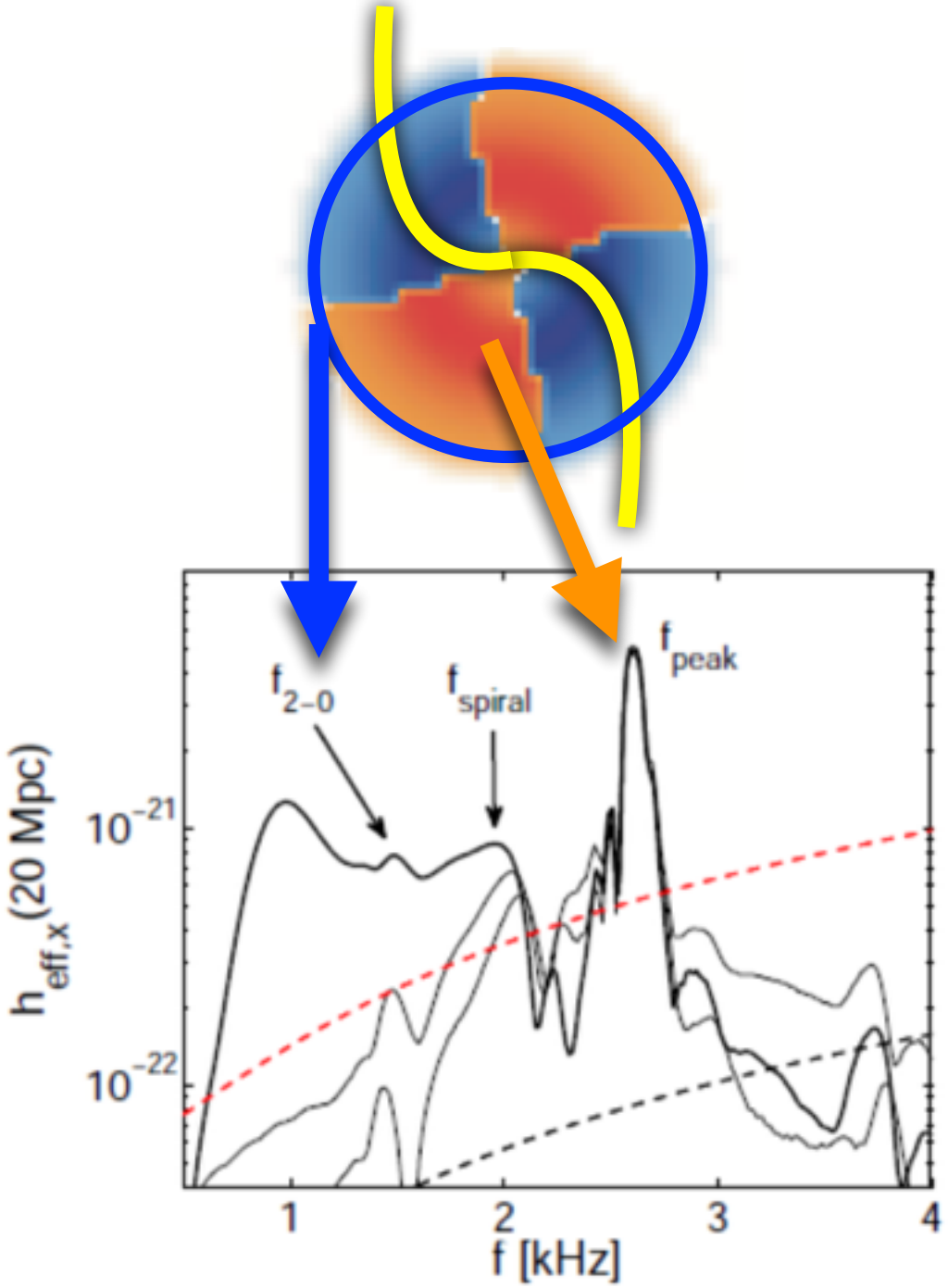

linear + quasi-linear + nonlinear

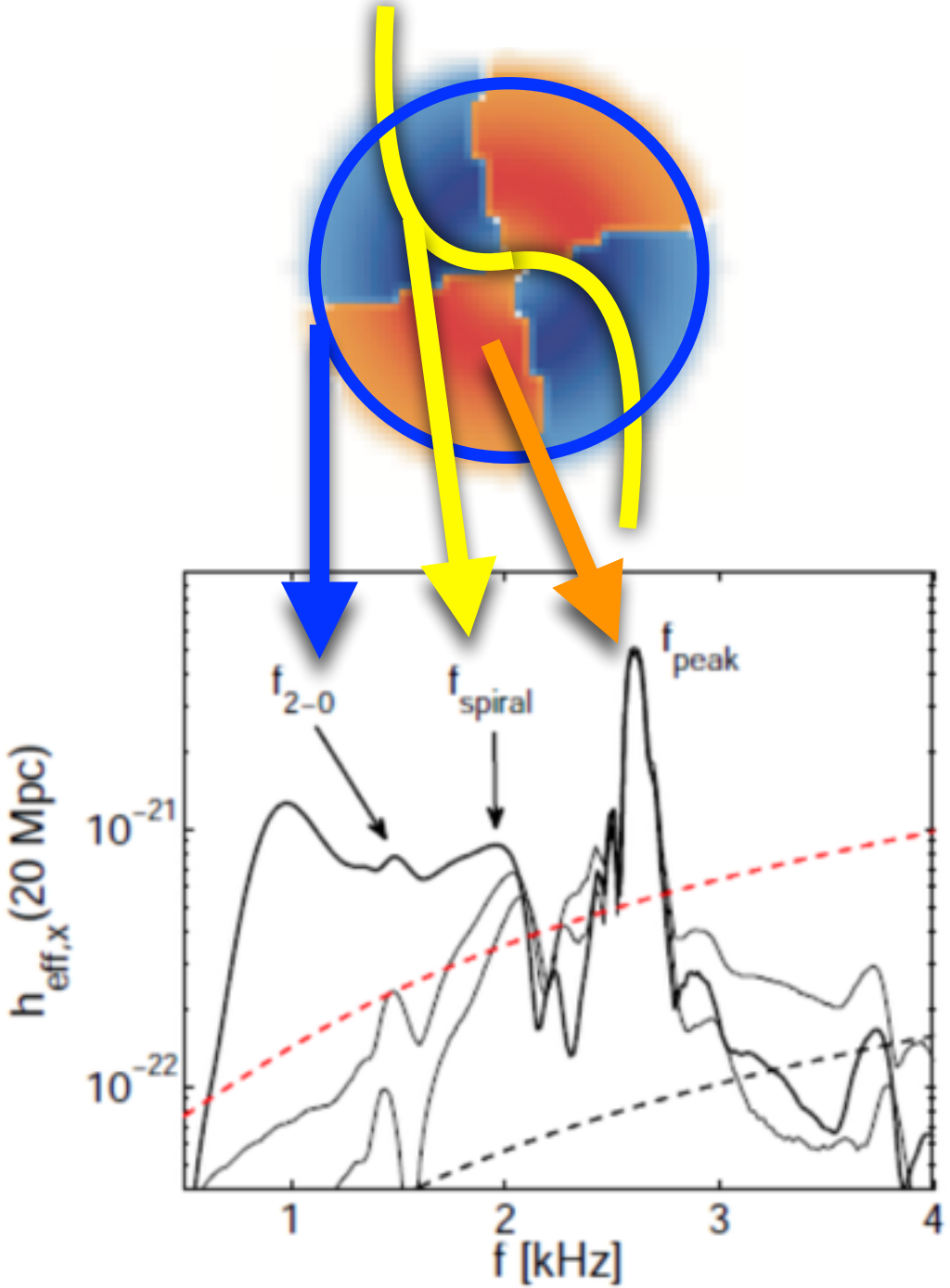

Three Types of Post-Merger Dynamics

Bauswein, NS (2015)

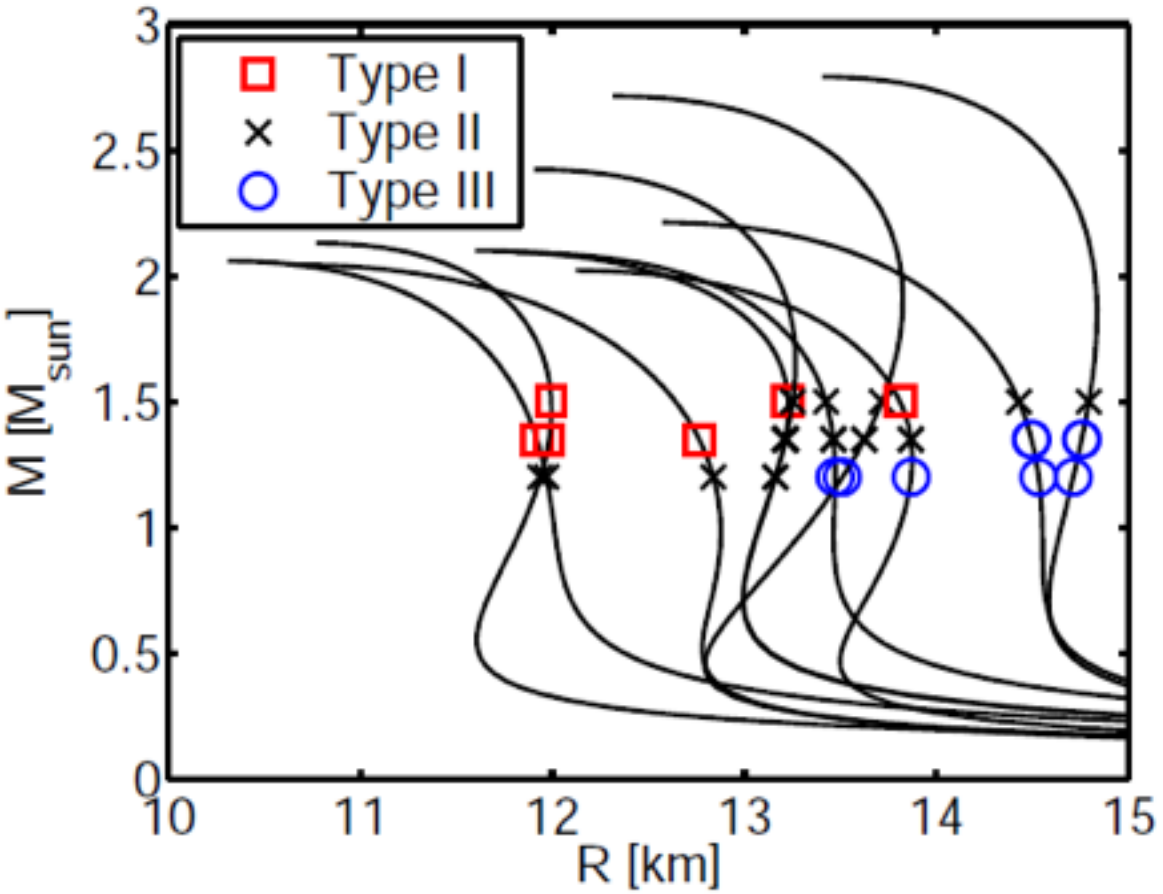

Type I: the "2-0" combination frequency dominates

Type II: **both** the "2-0" and the f_spiral frequencies are present

Type III: the f_spiral frequency dominates

Asteroseismology

Bauswein, NS (2015)

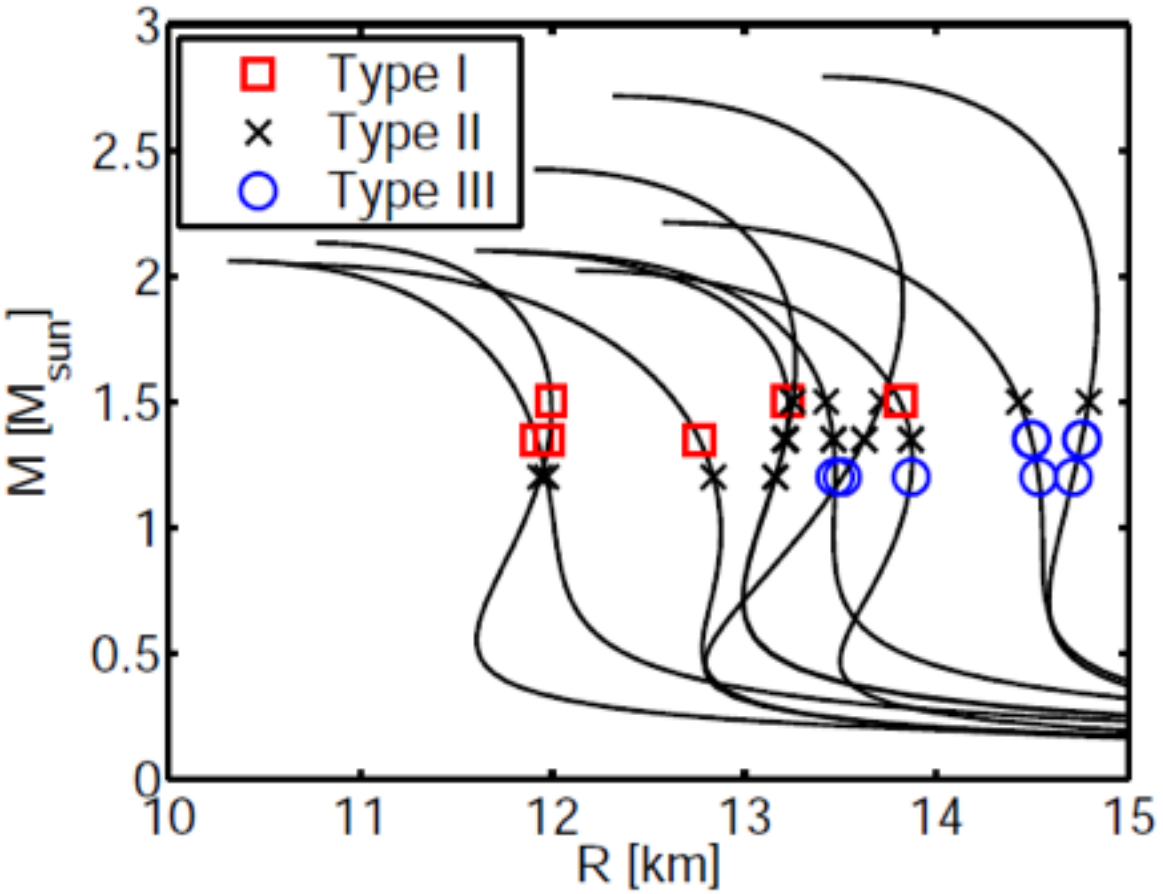

Type I: the "2-0" combination frequency dominates

Type II: **both** the "2-0" and the f_spiral frequencies are present

Type III: the f_spiral frequency dominates

GW Asteroseismology

Andersson & Kokkotas (1998)

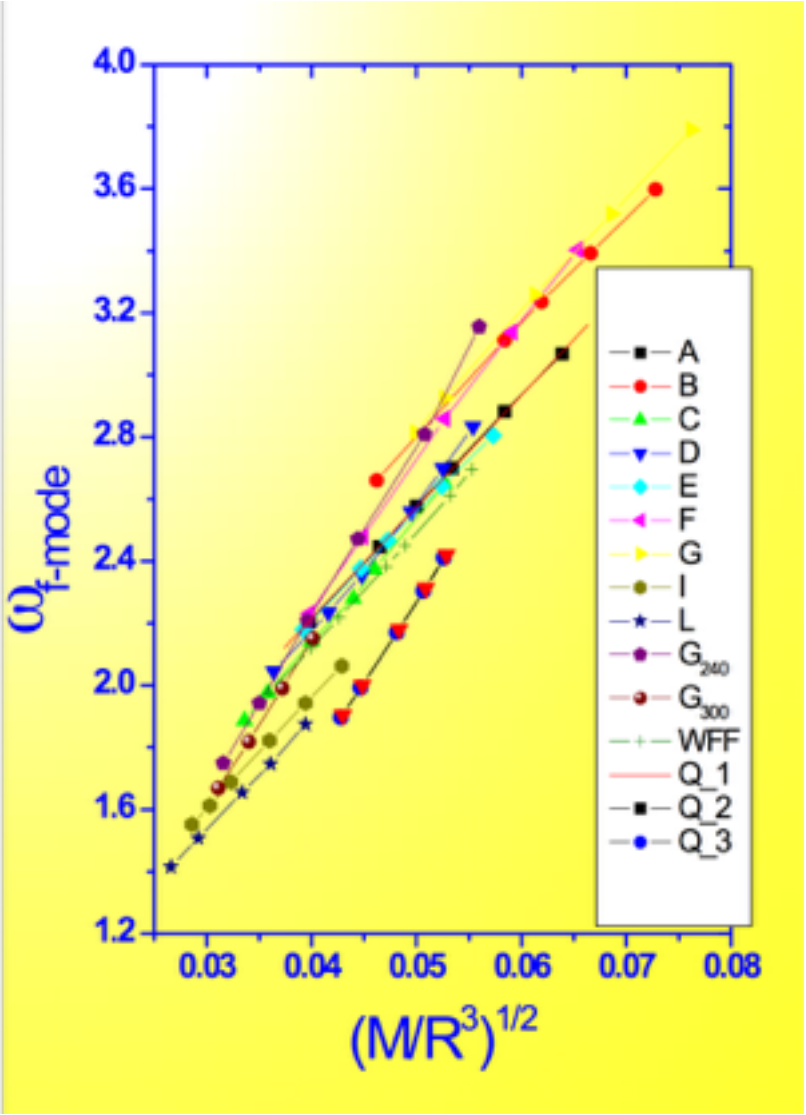

$$\omega_f\,(kHz) \approx 0.78 + 1.637\left(\frac{M_{1.4}}{R_{10}{}^3}\right)^{1/2}$$

Frequency-Radius Relation in BNS Remnants

Bauswein, Janka, Hebeler & Schwenk (2012)

f_{peak} correlates very well with the radius @ 1.6 Msun, if M_{tot} is known from inspiral.

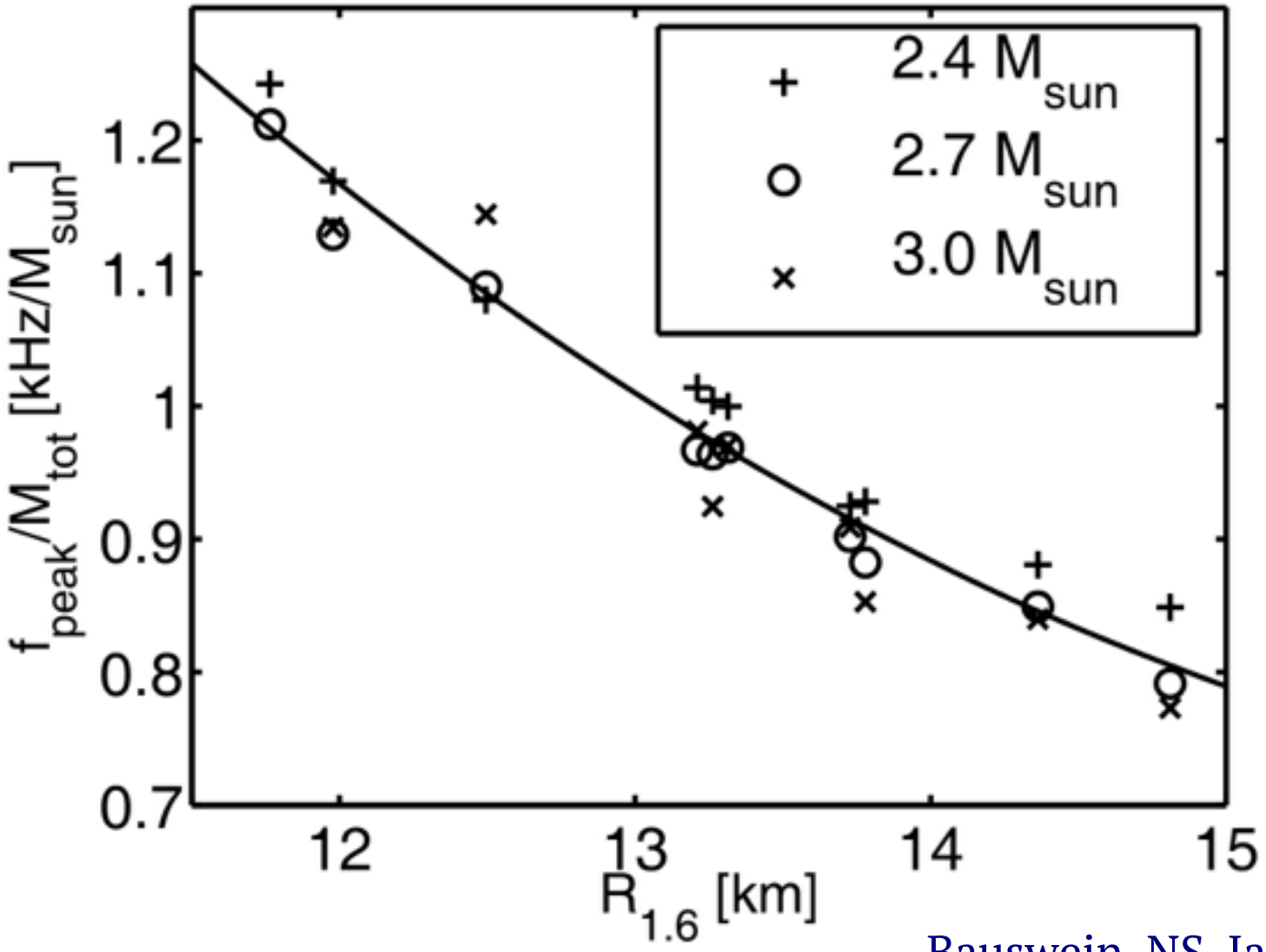

Bauswein, NS, Janka (2016)

Radius Determination from Post-Merger Signal

Bauswein, Janka, Hebeler & Schwenk (2012)

f_{peak} correlates very well with the radius @ 1.6 Msun, if M_{tot} is known from inspiral.

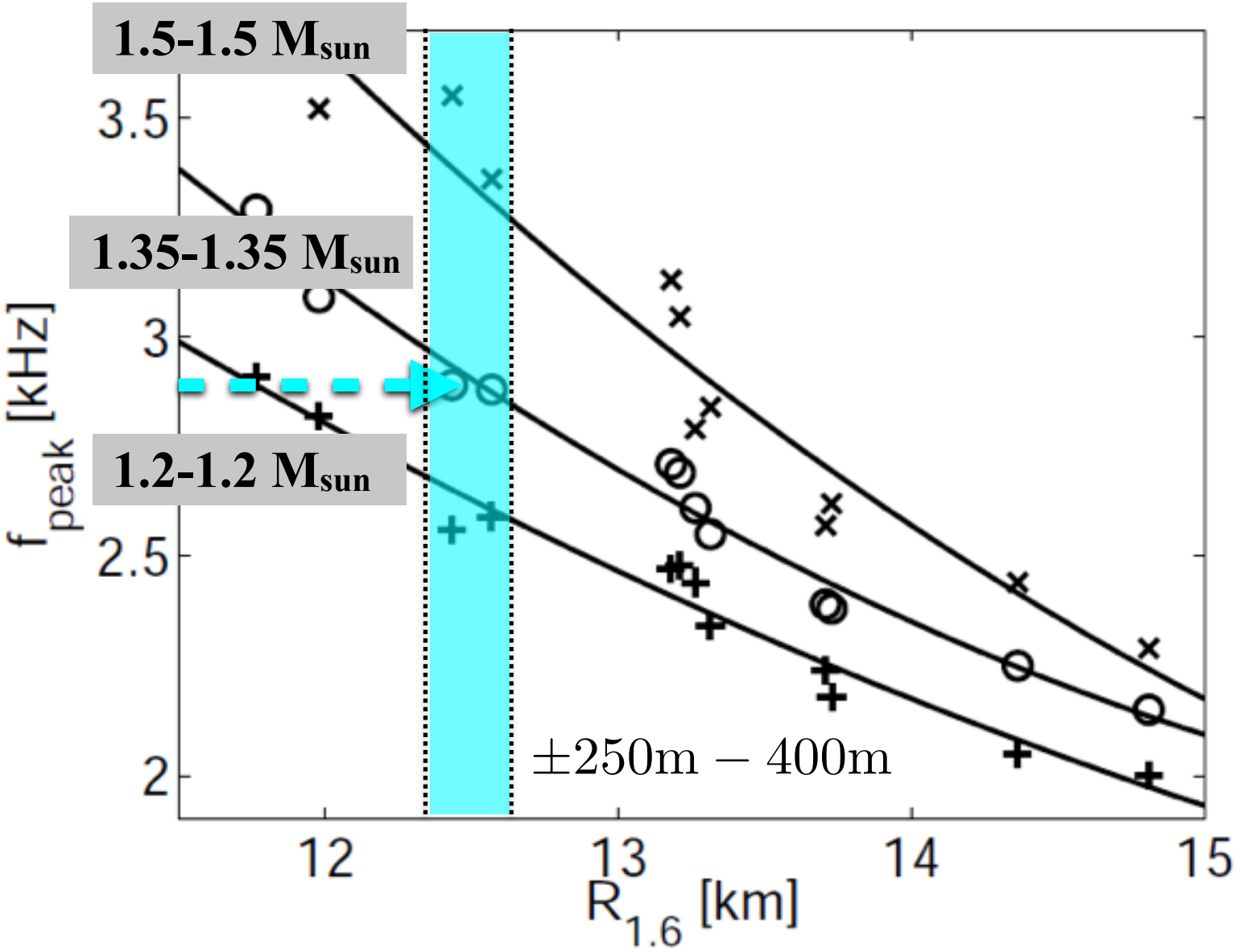

Revealing the EOS

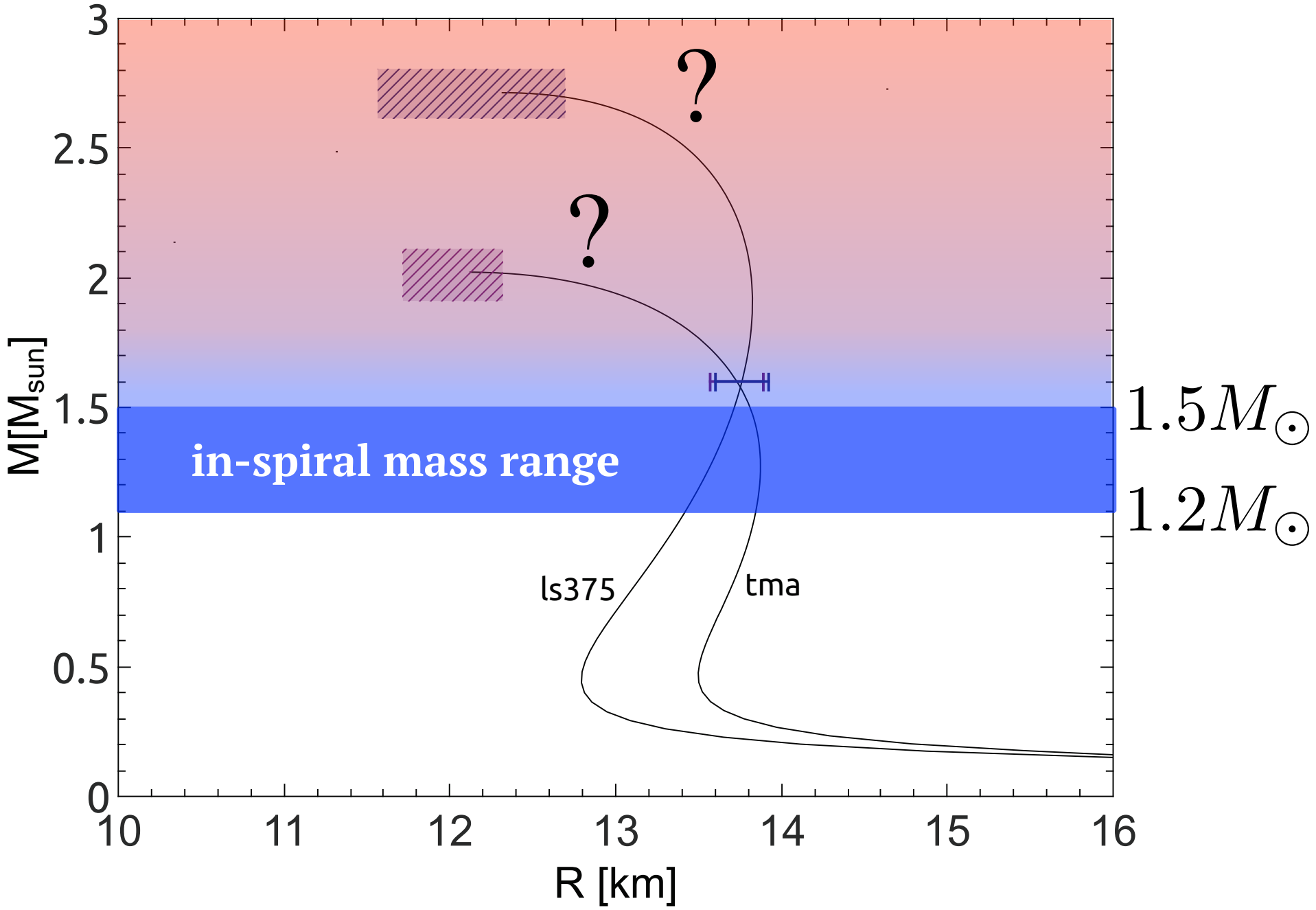

Extrapolating to Larger Masses

Bauswein, NS, Janka (2014)

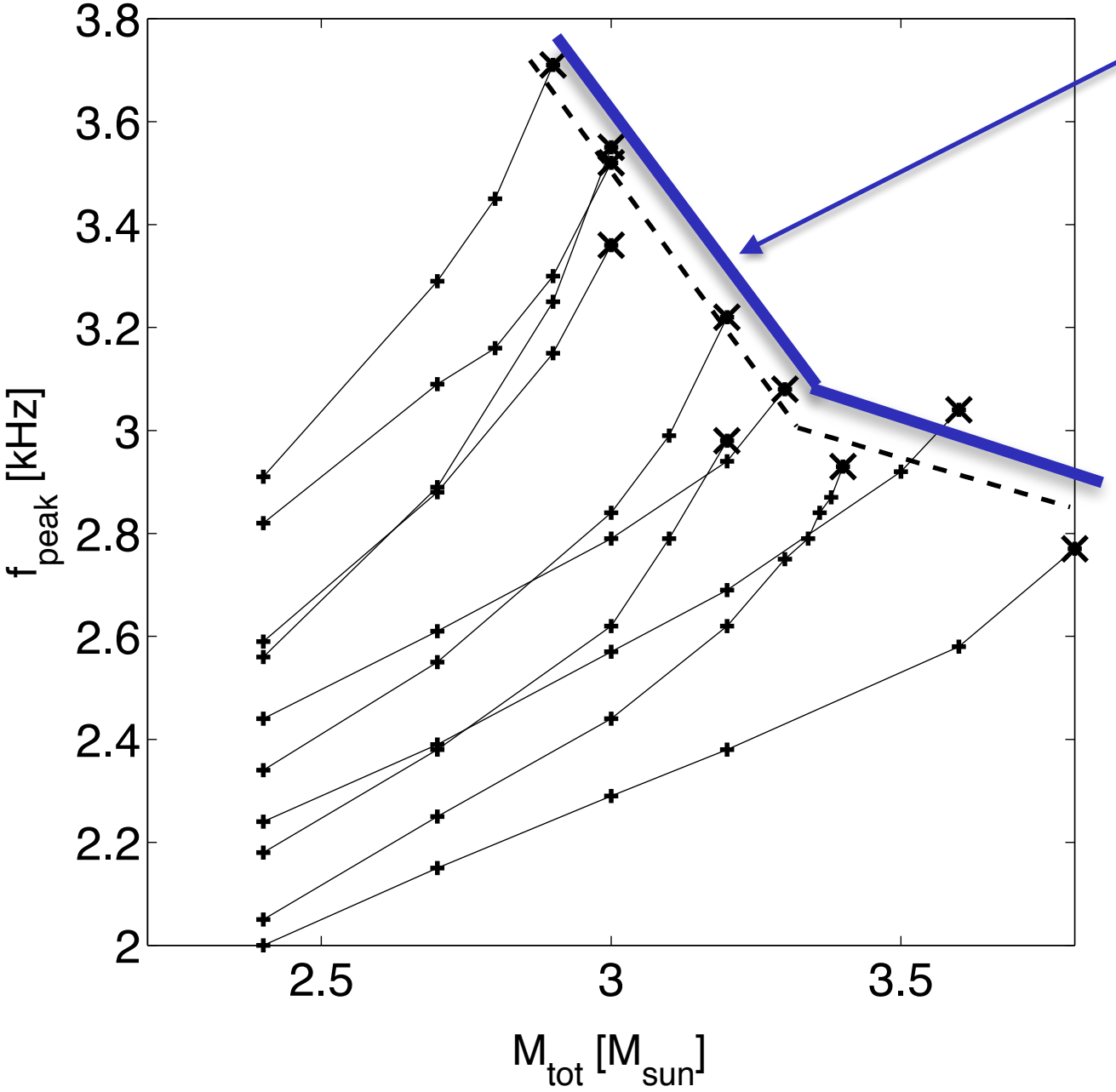

Extrapolating to Larger Masses

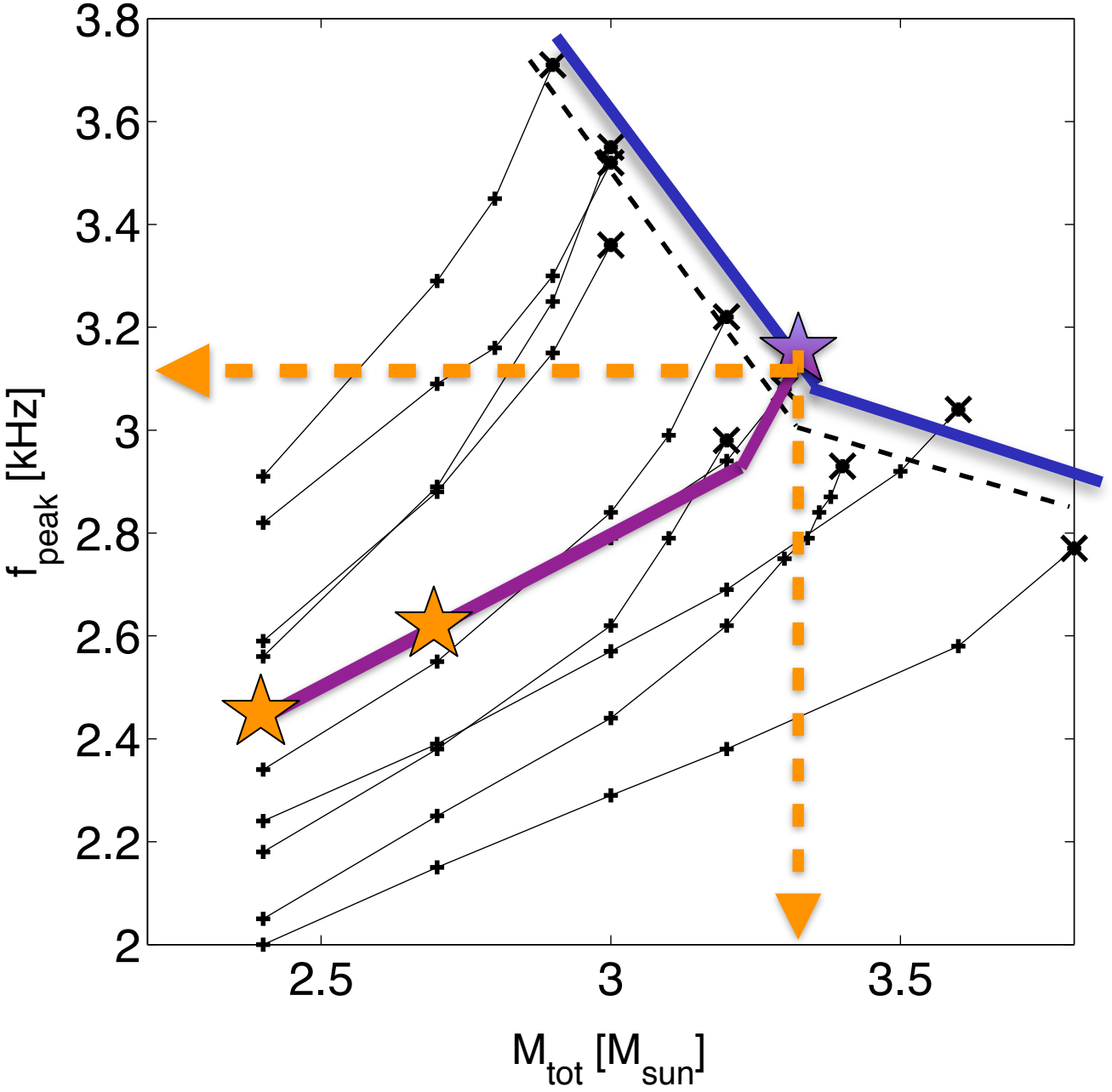

M_thres vs. M_max correlation

Bauswein, Baumgarte, Janka PRL (2013)

The threshold mass is related to the maximum TOV mass as

$$M_{\rm thres} = k \cdot M_{\rm max}$$

where *k* is dependent on the compactness.

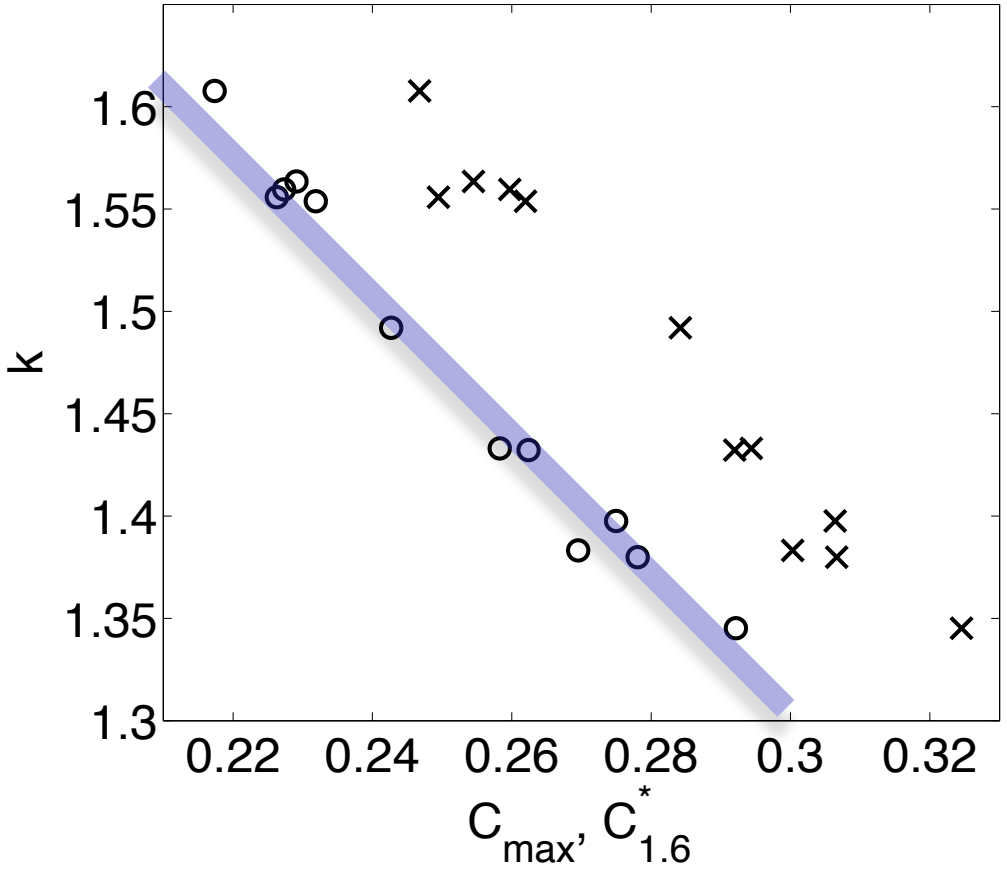

$$C_{\rm max} = (GM_{\rm max})/(c^2 R_{\rm max})$$

Breaking the EOS Degeneracy

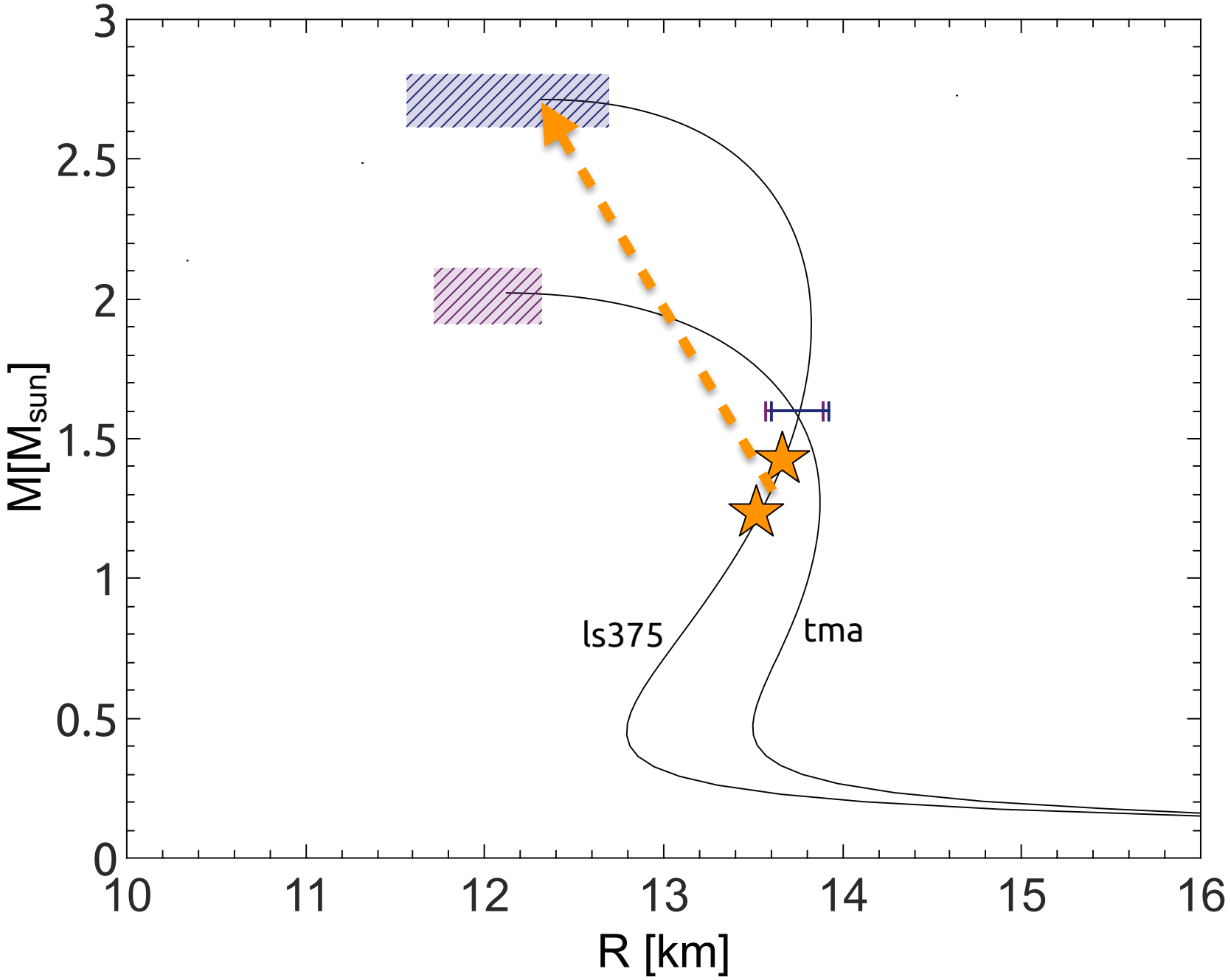

Detectability

Clark, Bauswein, NS, Shoemaker (2016)

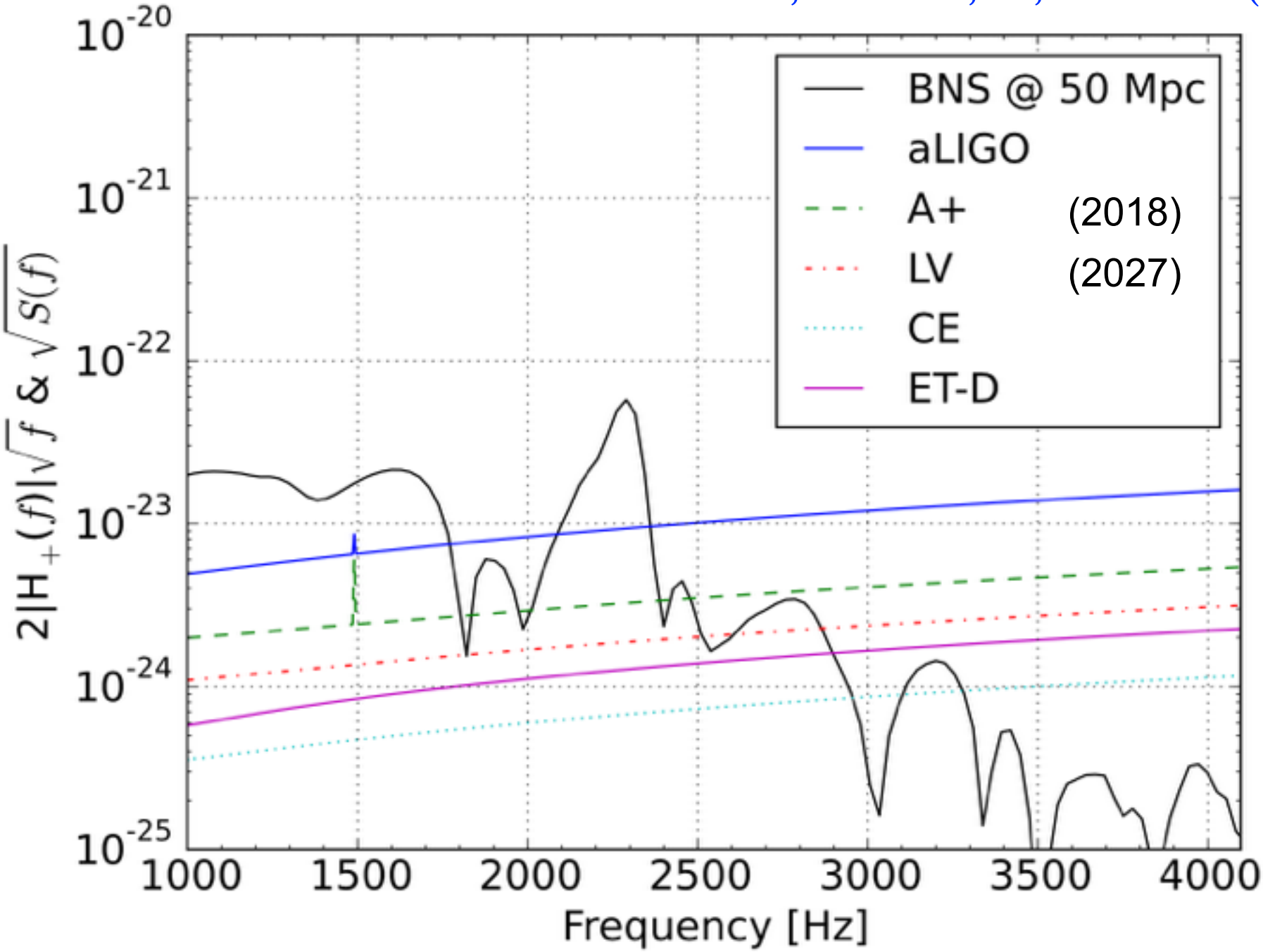

PLANNED UPGRADES AND NEW DETECTORS

Clark, Bauswein, NS, Shoemaker (2016)

LIGO A+ [74, 75] a set of upgrades to the existing LIGO facilities, including frequency-dependent squeezed light, improved mirror coatings and potentially increased laser beam sizes. Noise amplitude spectral sensitivity would be improved by a factor of $\sim$ 2.5-3 over 1–4 kHz. A+ could begin operation as early as 2017–18.

LIGO Voyager (LV) [75] a major upgrade to the existing LIGO facilities, including higher laser power, changes to materials used for suspensions and mirror substrates and, possibly, low temperature operation. LV would become operational around 2027–28 and offer noise amplitude spectral sensitivity improvements of $\sim$ 4.5-5 over 1–4 kHz.

LIGO Cosmic Explorer (CE) [75] a new LIGO facility rather than an upgrade, with operation envisioned to commence after 2035, probably as part of a network with LIGO Voyager. In its simplest incarnation, Cosmic Explorer would be a straightforward extrapolation of A+ technology to a much longer arm length of 40 km, referred to as CE1 which would be $\sim 14\times$ more sensitive than aLIGO over 1–4 kHz. An alternative extrapolation is that of Voyager technology to the 40 km arm length, referred to as CE2. CE2 is only $\sim 8\times$ more sensitive than aLIGO for the frequency range of interest in this study. For simplicity, we consider only CE1.

Einstein Telescope (ET-D) [76, 77] the European third-generation GW detector. In this work, we consider the ET-D configuration which is comprised of two individual inteferometers where one targets low frequency sensitivity and the other high frequency sensitivity. Both interferometers will be of 10 km arm length and housed in an underground facility. Furthermore, the full observatory will consist of three such detectors in a triangle arrangement. ET-D is $\sim 8\times$ more sensitive than aLIGO over 1–4 kHz. Due to the network configuration (i.e., the alignment of the component instruments) the effective sensitivity of ET-D is $\sim$ 18% higher than that for a single ET-D detector.

Expected Detection Rate

Clark, Bauswein, NS, Shoemaker (2016)

Single detector, ideal matched-filtering, SNR threshold=5

Instrument	SNR_{full}	D_{hor} (Mpc)	$\dot{\mathcal{N}}_{det}$ (year^{-1})
aLIGO	$2.99^{3.86}_{2.37}$	$29.89^{38.57}_{23.76}$	$0.01^{0.03}_{0.01}$
A+	$7.89^{10.16}_{6.25}$	$78.89^{101.67}_{62.52}$	$0.13^{0.20}_{0.10}$
LV	$14.06^{18.13}_{11.16}$	$140.56^{181.29}_{111.60}$	$0.41^{0.88}_{0.21}$
ET-D	$26.65^{34.28}_{20.81}$	$266.52^{342.80}_{208.06}$	$2.81^{5.98}_{1.33}$
CE	$41.50^{53.52}_{32.99}$	$414.62^{535.221}_{329.88}$	$10.59^{22.78}_{5.33}$

Coherent Wave Burst Analysis

Clark, Bauswein, Cadonati, Janka, Pankow, NS (2014)

A simple burst algorithm only recovers ~40% of the input signal.

Target (noise free)

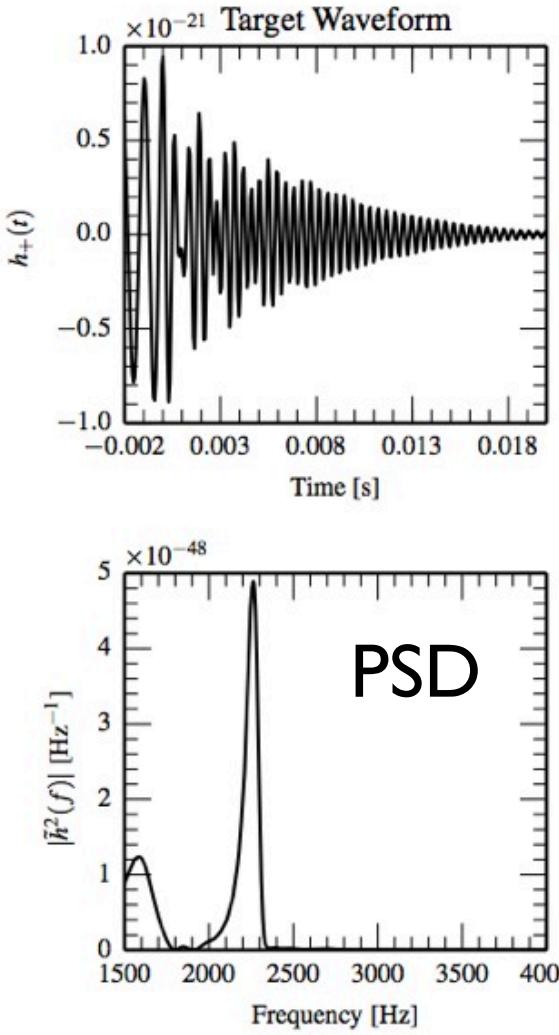

Reconstructions

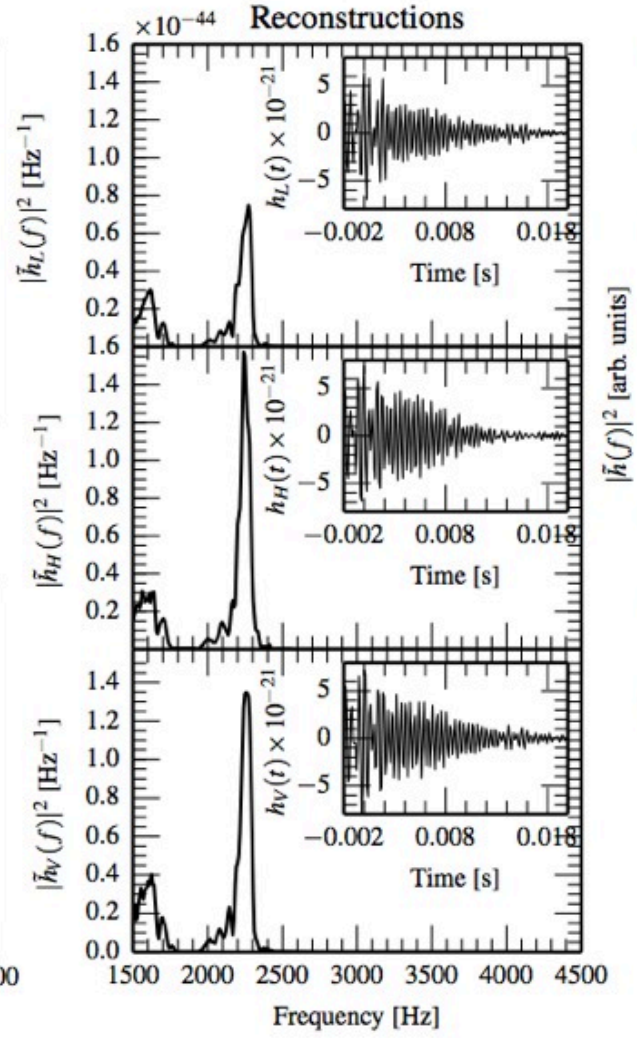

Fit to reconstructed spectrum

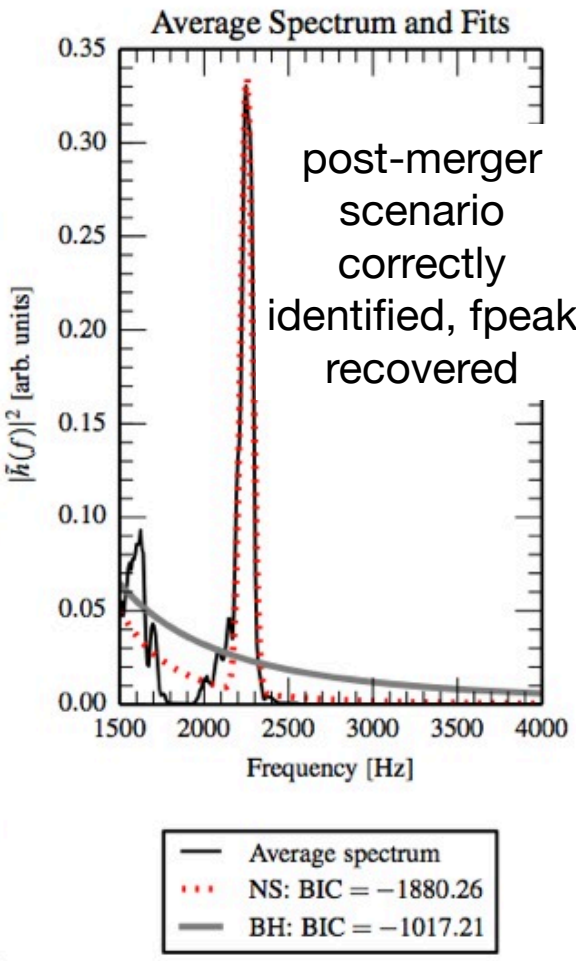

Principal Component Analysis (PCA)

Clark, Bauswein, NS, Shoemaker (2016)

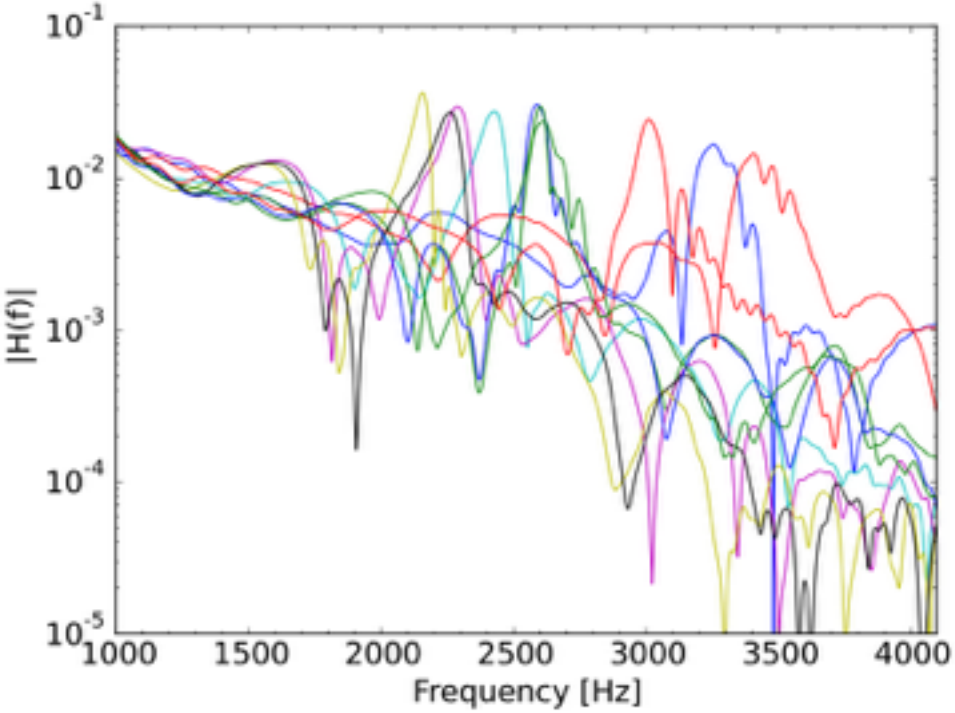

Actual fft's for different models.

Principal Component Analysis (PCA)

Clark, Bauswein, NS, Shoemaker (2016)

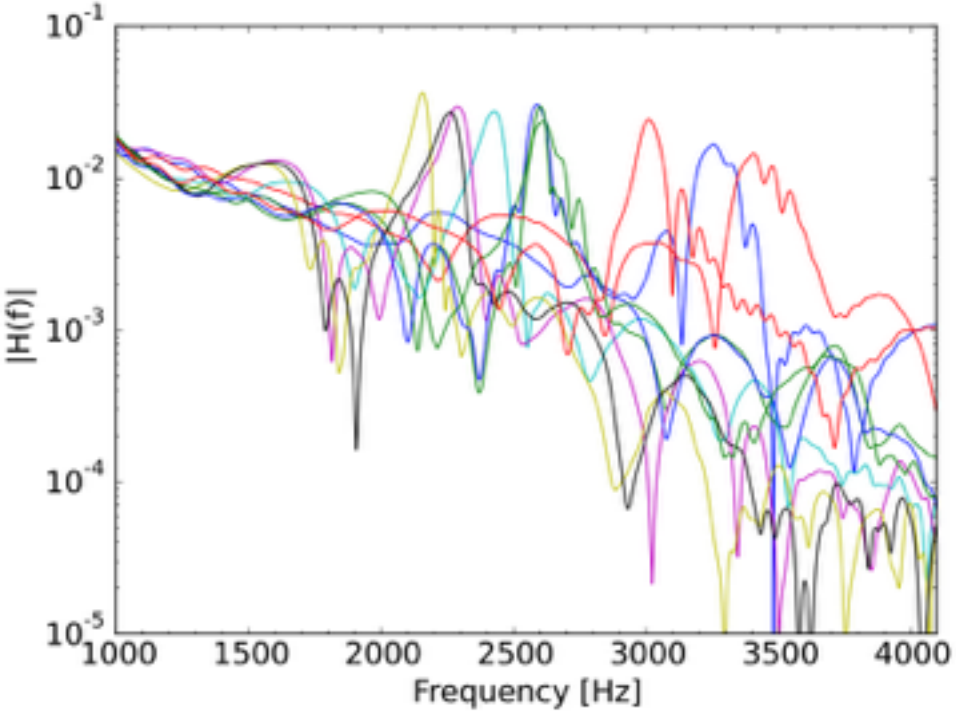

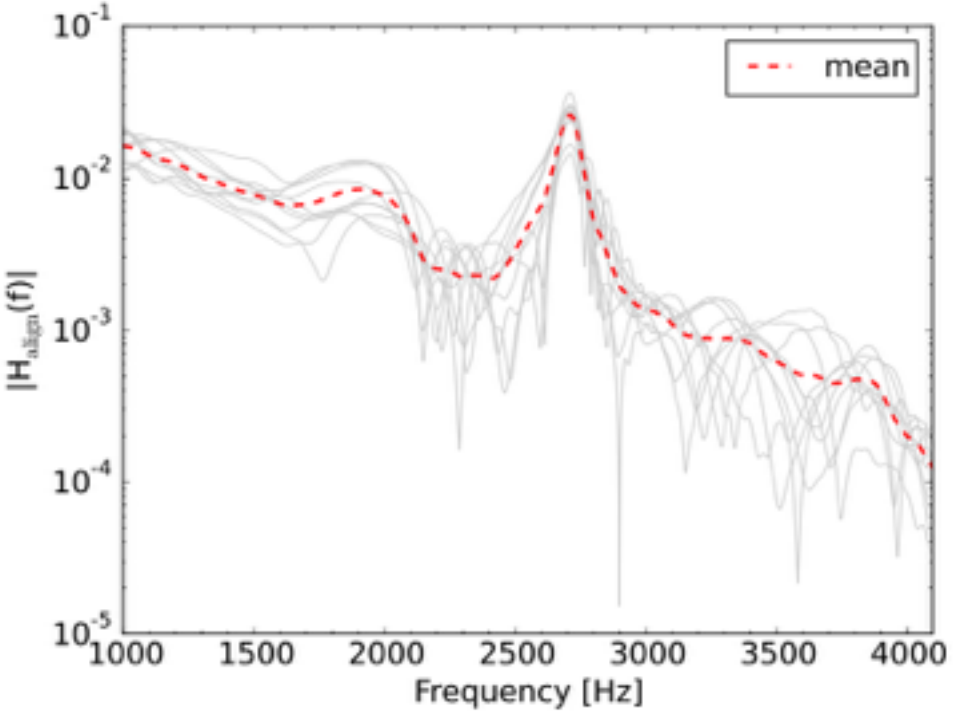

Actual fft's for different models.

Rescaled to common reference model.

Principal Component Analysis (PCA)

Clark, Bauswein, NS, Shoemaker (2016)

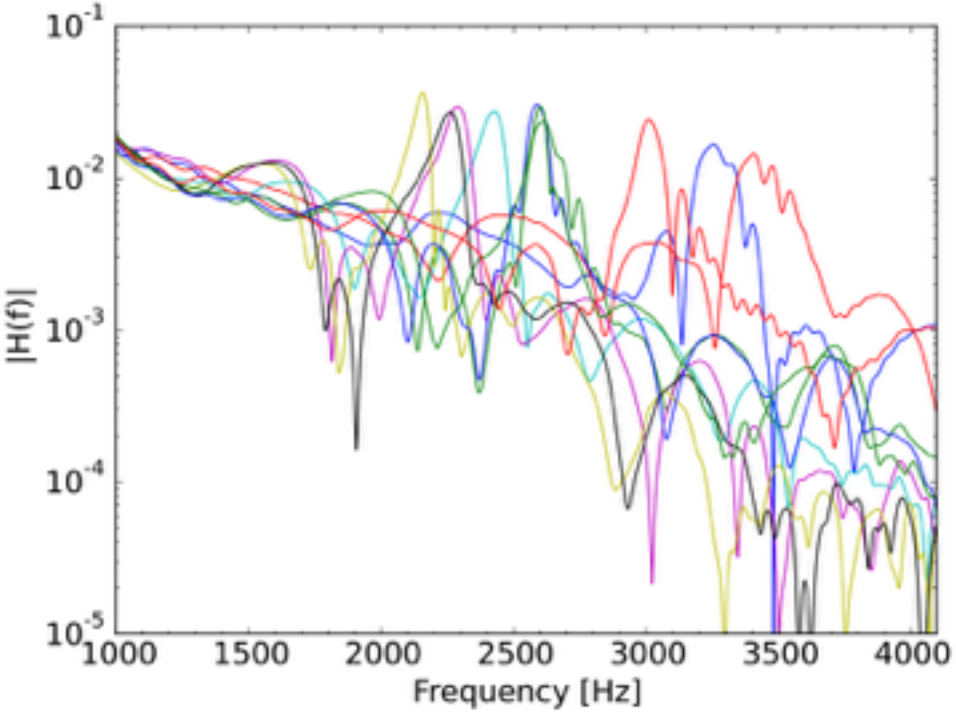

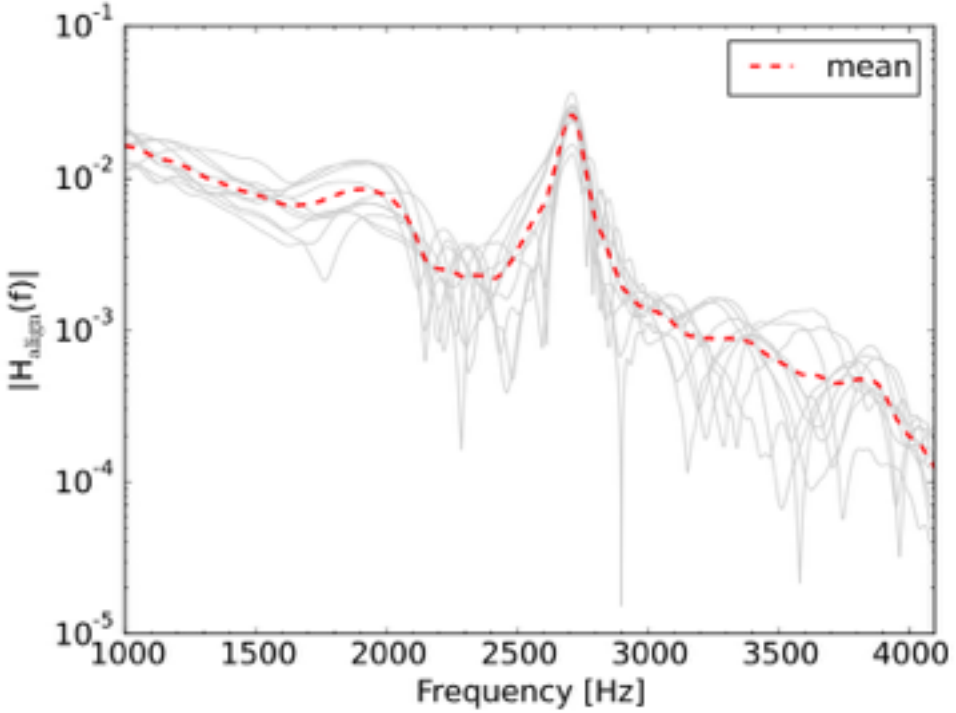

Actual fft's for different models.

Rescaled to common reference model.

Our PCA template extracts >90% of signal power compared to only 40% when using simple burst analysis.

PCA Reconstruction of signal

Clark, Bauswein, NS, Shoemaker (2016)

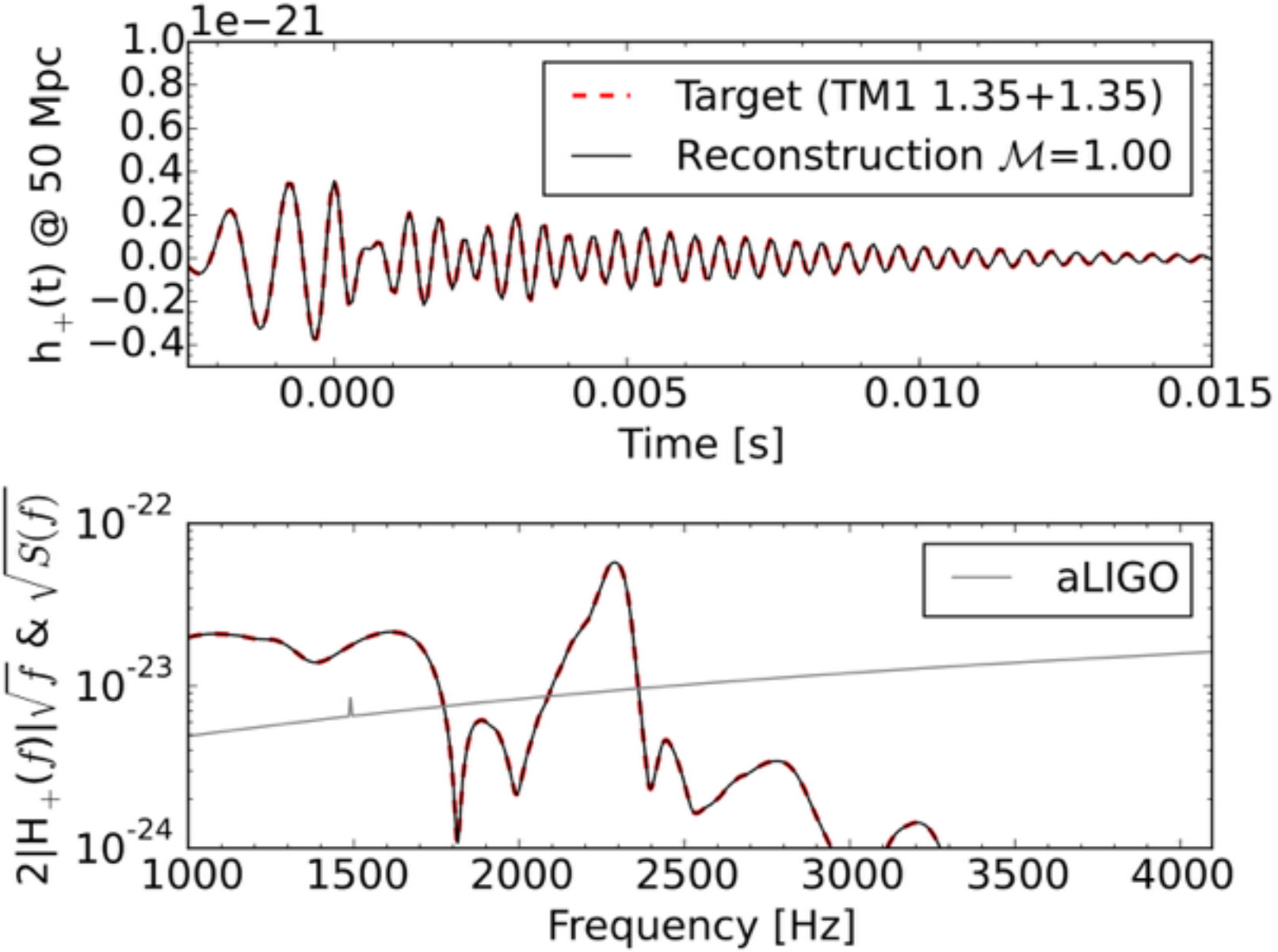

PCA Reconstruction of signal

Clark, Bauswein, NS, Shoemaker (2016)

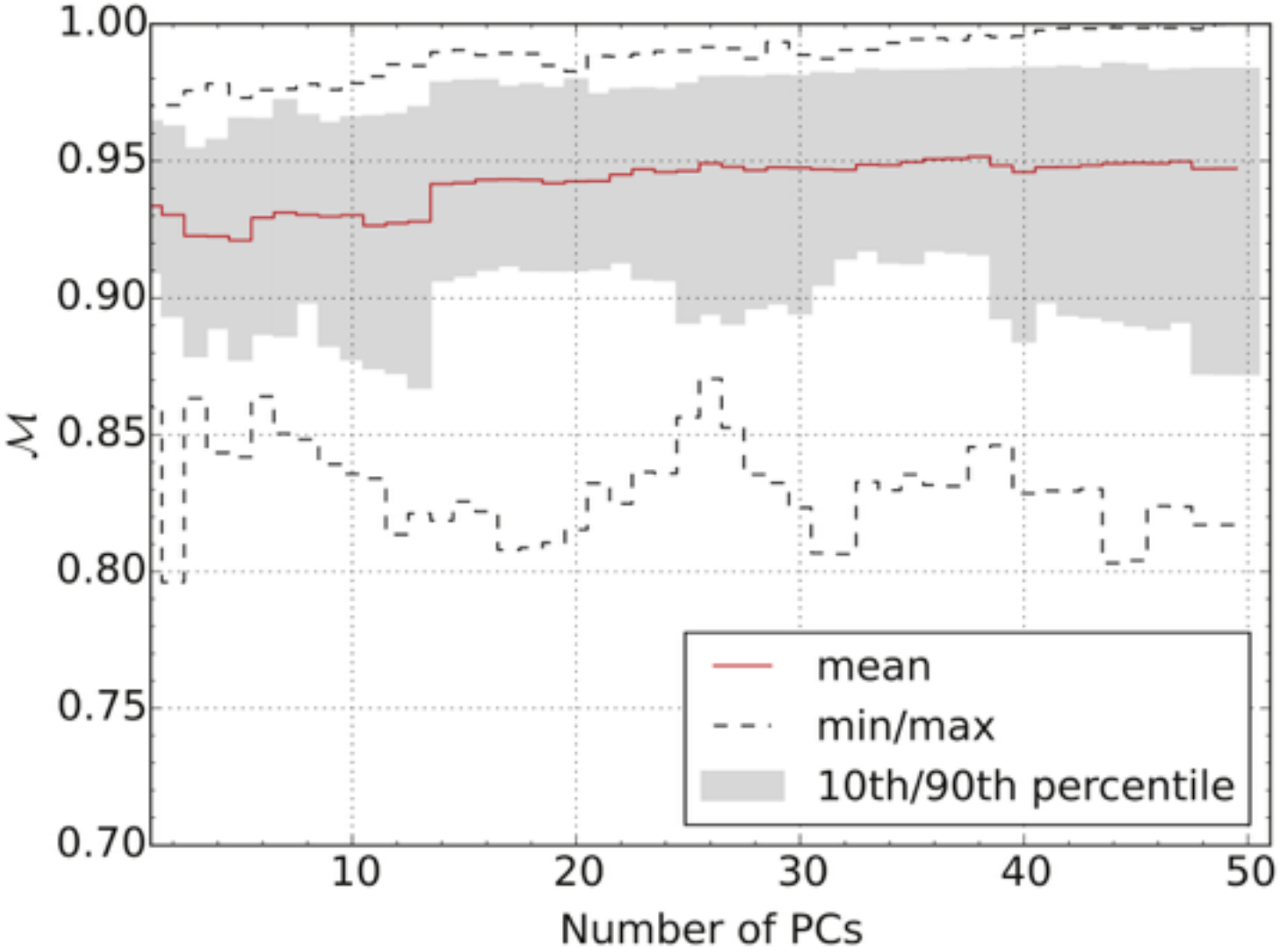

Our PCA template extracts >90% of input signal. Even with mean+1 PC, it is >80% (compared to 40% for a burst analysis).

Summary

- Post-merger GW asteroseismology is a viable method for constraining the EOS
- Neutron star radii can be measured to 400m (~3%) maximum uncertainty
- Principal Component Analysis (PCA) sufficient to reach >90% of optimal signal
- Realistic detection rates possible with upgraded LIGO Voyager by 2027.

THANK YOU!